Evaluating the Community Land Model in a pine stand with shading manipulations and $^{13}CO_2$ labeling

[Revised manuscript for Biogeosciences]

Jiafu Mao[1,*], Daniel M. Ricciuto[1], Peter E. Thornton[1], Jeffrey M. Warren[1], Anthony W. King[1], Xiaoying Shi[1], Colleen M. Iversen[1] and Richard J. Norby[1]

[1] Environmental Sciences Division and Climate Change Science Institute, Oak Ridge National Laboratory, Oak Ridge, Tennessee, USA

[*] Corresponding author: (Tel: +1-865-576-7815, maoj@ornl.gov)

Abstract. Carbon allocation and flow through ecosystems regulates land surface–atmosphere CO_2 exchange and thus is a key, albeit uncertain, component of mechanistic models. The Partitioning in Trees and Soil (PiTS) experiment-model project tracked carbon allocation through a young *Pinus taeda* stand following pulse-labeling with $^{13}CO_2$ and two levels of shading. The field component of this project provided process-oriented data that was used to evaluate terrestrial biosphere model simulations of rapid shifts in carbon allocation and hydrological dynamics under varying environmental conditions. Here we tested the performance of the Community Land Model version 4 (CLM4) in capturing short-term carbon and water dynamics in relation to manipulative shading treatments, and the timing and magnitude of carbon fluxes through various compartments of the ecosystem. When calibrated with pretreatment observations, CLM4 was capable of closely simulating stand-level biomass, transpiration, leaf-level photosynthesis, and pre-labeling ^{13}C values. Over the 3-week treatment period, CLM4 generally reproduced the impacts of shading on soil moisture changes, relative change in stem carbon, and soil CO_2 efflux rate. Transpiration under moderate shading was also simulated well by the model, but even with optimization we were not able to simulate the high levels of transpiration observed in the heavy shading treatment, suggesting that the Ball-Berry conductance model is inadequate for these conditions. The calibrated version of CLM4 gave reasonable estimates of label concentration in phloem and in soil surface CO_2 after three weeks of shade treatment, but lacks mechanisms needed to track the labeling pulse through plant tissues on shorter time-scales. We developed a conceptual model for photosynthate transport based on the experimental observations, and discussed conditions under which the hypothesized mechanisms could have an important influence on model

behavior in larger-scale applications. Implications for future experimental studies are described, some of which are already being implemented in follow-on studies.

1 Introduction

Accurate projection of the changing global climate, given a particular scenario of future greenhouse gas emissions or concentrations, is largely determined by adequate representation of mechanistic processes in Earth System Models (ESMs) (Taylor et al., 2012). Land Surface Models (LSMs) and their associated biogeophysical and biogeochemical parameterizations are key determinants of the ESMs' fidelity in characterizing and quantifying complex feedbacks in the Earth System (Arora et al., 2013; Friedlingstein et al., 2006; Pitman, 2003). Modeling studies have increasingly used observational data and mechanistic knowledge of processes to advance the development of LSMs (Best et al., 2011; Dai et al., 2003; Krinner et al., 2005; Oleson et al., 2013; Wang et al., 2011). Global and regional observations of land surface fluxes, states, and dynamic vegetation change offer insights into the large-scale interactions between the land surface and atmosphere, and hence facilitate model improvements at relevant scales in space and time (Beer et al., 2010; Huntzinger et al., 2012; Luo et al., 2012; Randerson et al., 2009). However, to better quantify and reduce uncertainties arising from deficiencies in model process representation, parameters, driver datasets and initial conditions, there has been significant effort to evaluate and to calibrate LSMs against site-scale observations and experimental manipulations (Baldocchi et al., 2001; De Kauwe et al., 2014; Hanson et al., 2004; Ostle et al., 2009; Raczka et al., 2013; Richardson et al., 2012; Schaefer et al., 2012; Schwalm et al., 2010; Stoy et al., 2013;

74 Walker et al., 2014; Williams et al., 2009; Zaehle et al., 2014). Further, model
75 development from these focused site-scale studies, especially in close collaboration with
76 experimentalists, can inform and prioritize new experiments and observations that are
77 specifically designed to advance understanding of critical terrestrial ecosystems and
78 processes (Shi et al., 2015).

79 The Community Land Model (CLM) is an advanced LSM with a comprehensive
80 mechanistic parameterization of carbon (C), water, and energy budgets for diverse land
81 types that can be applied across multiple temporal scales (Oleson et al., 2010). CLM has
82 been evaluated against observations from a wide range of sources, and these evaluations
83 have resulted in improved model performance (Bauerle et al., 2012; Bonan et al., 2011,
84 2012; Koven et al., 2013; Lawrence et al., 2011; Mao et al., 2012a, 2012b, 2013; Oleson
85 et al., 2008; Randerson et al., 2009; Riley et al., 2011; Shi et al., 2011, 2013, 2015;
86 Thornton et al., 2007). Nevertheless, little attention has been paid to CLM's ability to
87 replicate short-term manipulative experiments, which provide an avenue for exploring
88 and validating model response to sudden, large changes in environmental drivers that
89 control physiological and ecological responses (Amthor et al., 2001; Bonan et al., 2013).
90 Processes operating over short time scales can have long-lived ecosystem consequences
91 through indirect effects; e.g., stomatal conductance varies on timescales of hours or
92 shorter, but indirect effects on site-level water balance through controls on transpiration
93 can extend to annual timescales and beyond. Combined model-experiment projects can
94 focus efforts on specific mechanistic processes whose representation in the model may be
95 neither adequate nor appropriate for specific sites (Walker et al., 2014; Zaehle et al.,
96 2014). Extending these model-experiment evaluations and ensuing model refinements to

97 additional sites of the same and different ecosystem types improves confidence in the
98 regional and global scale adequacy of the LSM's mechanistic process representation and
99 parameterization.

100 Photosynthetic C assimilation, the allocation of photosynthetic products into
101 tissues with different turnover rates, and the respiration of C back into the atmosphere
102 areimportant determinants of CO_2 exchange between the terrestrial biosphere and the
103 atmosphere (Schimel et al., 2001). Biosphere-atmosphere C exchange is dynamically
104 mediated by weather, soil conditions, vegetation community composition and phenology,
105 and natural and anthropogenic disturbances (Cannell and Dewar, 1994; Litton et al.,
106 2007). Mechanistic characterization of the fate of photosynthetically-fixed C, in
107 particular the magnitude and timing of C allocation among plant compartments, is a
108 major challenge for experimental and modeling communities (Epron et al., 2012).
109 Various C-allocation schemes have been proposed and implemented in LSMs to capture
110 both the dynamic changes in C allocation and response to external conditions of C
111 allocation (De Kauwe et al., 2014). They generally employ either fixed coefficients or in
112 some cases dynamic coefficients that are functions of time or time-varying external
113 conditions to allocate assimilated C to different plant components (e.g., leaves, stems,
114 and roots). These allocation schemes and coefficients are generally not well constrained
115 by observations. More process-based understanding, better measurement techniques, and
116 targeted experimental manipulations are needed to better constrain allocation within the
117 model structure and the models' representations of C dynamics.

118 Carbon isotopes provide important constraints on specific processes and can be
119 used in labeling experiments to track pulses of carbon through plant and soil components.

120 Both diffusion through stomata and enzyme activity during photosynthesis discriminate
121 against the accumulation of ^{13}C in plant tissue, making ^{13}C measurement a useful
122 constraint on stomatal conductance (Farquhar et al., 1989). Exposing plants to ^{13}C
123 enriched CO_2 can provide important constraints on simulated C allocation (Ehleringer et
124 al., 2000). The post-treatment carbon isotope composition ($\delta^{13}C$) of organic matter and
125 respired CO_2 can serve as a tracer of plant C allocation (Atkin 2015; Bahn et al., 2012).
126 We evaluated the integrated response of a simulated tree-soil system to an
127 imposed alteration of shortwave radiation, the main environmental driver for
128 photosynthesis, and compared the observed trajectory of labeled carbon pulses through
129 that system with approximations of carbon allocation that are typical of a global-scale
130 model. We used a version of CLM4.0 that has been modified to allow convenient
131 application of the global-scale modeling algorithms at single points (PTCLM, described
132 in Oleson et al., 2013). We evaluated the model against observations and experimental
133 results from the "Partitioning in Trees and Soils" (PiTS) experiment established in a
134 young loblolly pine stand in Oak Ridge, Tennessee, USA (Warren et al., 2013). The
135 project exposed a young loblolly pine (*Pinus taeda*) stand to a pulse of air enriched with
136 $^{13}CO_2$, then tracked that label from photosynthetic uptake, through the leaves, stem, and
137 roots and ultimately out of the soil as respiratory flux photosynthetically active radiation
138 (PAR) (Warren et al., 2012). We addressed two questions: (i) Is the model able to
139 represent the biophysical and ecophysiological behavior of the experimental system in
140 terms of pretreatment dynamics and stand-level response to the manipulated radiation
141 environment? (ii) Do the biases inherent in a very simple model of storage and allocation
142 propagate beyond the time scale of fast turnover storage pools? We hypothesized that it

143 would be possible to parameterize the global model using site-level ecophysiological
144 measurements, and have it realistically capture the site-level influence of the shade
145 manipulation. We further hypothesized that, in spite of missing mechanisms to track
146 short-term storage and allocation of C, the parameterized model could capture both
147 pretreatment ^{13}C discrimination as well as post-treatment effects once the labeling pulse
148 had traveled through the plant.
149

150 2 Methodology

151 2.1 Site description, experimental manipulation, and observations

152 The field component of the project was conducted in a young loblolly pine stand at the
153 University of Tennessee Forest Resources AgResearch and Education Center in Oak
154 Ridge, Tennessee. The soil is classified as a silt-clay-loam (13.3% sand; 35.7% clay;
155 51.0% silt), with bulk density ranging from 1.2 to 1.4 g cm^{-3} at 10 to 70 cm depth. One-
156 year-old seedlings (1 g C m^{-2} (Griffin et al., 1995)) were planted at 2.5 × 3 m spacing in
157 2003, and the experiment was conducted in 2010 when the trees were ~7 m tall.
158 In 2010, a subset of eight of the trees, adjacent to one another, and their soils, were
159 instrumented with automated sensors to continuously measure soil temperature, soil
160 moisture vertically throughout the soil profile, soil surface $^{12}CO_2$ and $^{13}CO_2$ efflux, root
161 production at 10 and 30 cm depths, stem sap flow, and stem diameter (Warren et al.,
162 2012). Various measurements were manually collected periodically, including predawn
163 foliar water potential, photosynthetic light- and CO_2-response curves, root biomass,
164 growth, and mortality, and soil C and nutrient content. Meteorological data were
165 collected every 30 minutes at 2 m height in an adjacent open field, and included wind

166 speed, air temperature, photosynthetically active and shortwave radiation, precipitation,
167 and relative humidity.
168 Following several weeks of pretreatment measurements, the eight study trees
169 were enclosed with plastic film stretched over a frame surrounding the trees, and then
170 trees were exposed to 53 liters of 99 atom % $^{13}CO_2$ for 45 minutes. The plastic was
171 removed and replaced with light shade (LS) or heavy shade (HS) cloth, each of which
172 covered four trees and provided differential levels of PAR at the canopy surface for 3
173 weeks following the labeling. The LS and HS cloths were designed to allow passage of
174 70% and 10%, respectively, of the incident PAR.
175 To assess actual conditions under the shade cloth treatments, short-term
176 measurements of temperature, humidity, wind speed, and PAR were collected at the
177 canopy surface following shade cloth installation. Linear regressions between
178 meteorological data from under the shade cloth and from the open field were used to
179 estimate conditions at the canopy surface during the experimental period. Temperature
180 was ~0.11°C (± 0.82 °C; ± 1 *SD*) lower, relative humidity (H_r) was ~6% (± 5%; ± 1 *SD*)
181 higher, and wind speed (u) was ~45% (± 15%; ± 1 *SD*) lower, under both levels of
182 shading than in the adjacent open field (Fig. 1a, b). The shade cloths performed very
183 close to design, with 68% and 11% passage of PAR through the LS and HS cloths,
184 respectively (Fig. 1c).
185 Non-destructive measurements of soil moisture, soil temperature, soil respiration,
186 sap flow and stem growth were made prior to the labeling and for the duration of the
187 shade treatment. During the shade treatment, destructive measurements of foliage, stem
188 phloem tissue, roots and soil were collected to assess presence of the ^{13}C label, and linked

189 to concurrent automated measurements of $^{13}CO_2$ from the soil surface (Warren et al.,
190 2012). Experimental results and additional details on the site and experimental design are
191 in Warren et al. (2012) and datasets are available online (Warren et al., 2013).

192 2.2 Model description

193 We used CLM4 (Oleson et al., 2010), the land component of the Community Earth
194 System Model (CESM) (Gent et al., 2011), to simulate the pretreatment and manipulated
195 processes in the PiTS study. This CLM version includes fully prognostic carbon and
196 nitrogen representations for its vegetation, litter, and soil biogeochemistry components
197 (Oleson et al., 2010, 2013; Thornton et al., 2007; Thornton and Rosenbloom, 2005).
198 Carbon allocation in this version of CLM is simplistic. After maintenance
199 respiration demands are calculated and subtracted from gross primary productivity
200 (GPP), and following a step that downregulates GPP on the basis of static allocation
201 parameters, fixed tissue C:N stoichiometry, and plant mineral N uptake, the available
202 carbon is allocated to new growth, storage for growth in subsequent growing seasons, and
203 associated growth respiration. The model includes pools for leaf, fine root, and several
204 categories of stem and coarse root, with over-season storage pools associated with each
205 of these "displayed" growth pools. The allocation ratio between stem and leaf is a
206 function of the previous year's net primary productivity (NPP; higher fractional
207 allocation to stem with higher annual NPP), while all other allocation ratios are fixed
208 throughout the simulation for a given vegetation type. For ^{13}C, stomatal diffusion and
209 photosynthetic fractionation are calculated and photosynthetically fixed ^{13}C is
210 immediately allocated to plant pools following the above description. There is no further
211 fractionation in within-plant processes or during decomposition (Oleson et al., 2013).

212 Several major developments of CLM performed specifically for this study
213 include: (1) introducing the ability to represent the shade effect and experimental labeling
214 by driving the model with observed atmospheric $^{13}CO_2$ concentrations, where before
215 $^{13}CO_2$ was assumed to be a constant fraction of CO_2, (2) developing a site-level
216 simulation workflow that leverages PTCLM capability to reproduce actual field
217 experiments, (3) calibration of the selected model parameters to improve predictions and
218 reveal structural errors, and (4) adding a stand-alone testing capability for the
219 photosynthesis subroutines.

220 2.2.1 Description of PTCLM simulation

221 To perform simulations at the PiTS site, we used PTCLM, a scripting framework to run
222 site-level simulations of CLM efficiently with site-specific forcing and initialization data
223 (Oleson et al., 2013). We performed the standard 600 years of accelerated decomposition
224 spinup, in which soil organic matter decomposition rates are increased (Thornton and
225 Rosenbloom, 2005), followed by 1000 years of normal spinup, in which the
226 decomposition rates are returned to their normal values, and a transient simulation
227 between 1850-2010 using historically varying CO_2, $^{13}CO_2$, nitrogen deposition, and
228 aerosol forcing data. Long-term meteorological driver data were not available at the PiTS
229 site, and instead were taken from the nearby Walker Branch and Chestnut Ridge eddy
230 covariance sites (Hanson et al., 2004) for the years 2000-2010. These input data were
231 cycled continuously to drive the model through the spinup and transient simulations. On
232 model date 1 January 2003, we simulated a harvest disturbance by removing existing
233 vegetation biomass and simulating planting of seedlings using a biomass of 1 g C m^{-2}.
234 The model then simulated growth of the young stand through the year 2010. For the

spinup and transient phases through 2002, default temperate evergreen needleleaf model parameters were used. Beginning in 2003, model parameters were modified to simulate the planted loblolly trees, based on ecophysiological measurements and model calibration (see Section 2.2.2).

To simulate the treatment period, we replaced the meteorology from the eddy covariance sites with observed data at the treatment sites starting at day of $^{13}CO_2$ labeling in September 2010 (Warren et al., 2012). The $^{13}CO_2$ pulse was applied in the model (assuming 100% $^{13}CO_2$) during a time matching the labeling period. Thermal infrared camera measurements under both light and heavy shade cloth made during various sky conditions indicated the need to modify the model input for incoming longwave radiation under the heavy shade treatment, by assuming that the heavy shade cloth emitted downward longwave at a blackbody temperature equal to the open field air temperature (data not shown). For the light shade case, we applied the model's internal estimate of incoming longwave radiation, which uses clear-sky assumptions about atmospheric temperature and emissivity (Idso, 1981).

2.2.2 Model calibration for pre- and post-treatment periods

Model evaluations are complicated by the co-occurrence of parametric and structural uncertainty, which confounds the attribution of model errors (Keenan et al., 2011). A model's performance might be negatively impacted by misrepresentation of mechanistic processes, poor parameterization of otherwise sound functional representations, or both. Parameter optimization, however, can help to isolate structural deficiencies in the model. In this study, we applied model calibration, by optimizing model parameters, as a tool to highlight areas for model development rather than simply improving predictive skill. We

258 optimized selected CLM parameters against pretreatment data. We then evaluated the
259 performance of the calibrated CLM in the pretreatment phase and again in the post-
260 treatment phase without recalibration following simulation of the canopy shading and
261 $^{13}CO_2$ treatments. Our intention is that by applying robust parameter optimization to the
262 pretreatment simulations we will reduce parametric uncertainty (Fox et al., 2009;
263 Ricciuto et al., 2011), leading to greater insight regarding model structural uncertainty in
264 evaluation of the post-treatment results.

265 We first calibrated the model to simulate the pretreatment conditions using
266 observations and prior information about model parameters. Data constraints for the
267 calibration consisted of single pretreatment estimates for leaf, stem, and root biomass
268 from allometric relationships for similarly aged loblolly pine (Baldwin, 1987; Naidu et
269 al., 1998; Vanlear et al., 1986), a pretreatment $\delta^{13}C$ measurement for leaves, a
270 pretreatment $\delta^{13}C$ measurement for bulk roots, and daily sap flow and soil respiration
271 observations from each of the 20 days preceding the $^{13}CO_2$ labeling and shading
272 treatments. Because CLM predicts canopy transpiration but not sap flow, daily
273 transpiration during the experiment was estimated by scaling the sap flow measurements
274 using sapwood area and ground area covered by the rooting system (Wullschleger et al.,
275 2001; Warren et al., 2011). Here we assume the rooting system of each tree occupied 7.5
276 m^2 of ground area based on the spacing between the trees. For consistency, sap flow is
277 hereafter called transpiration for both the observational and modeled results.

278 Some model parameters were specified directly from observations (Table 1).
279 Other parameters for which direct estimation was not possible were optimized to
280 maximize fit between model results and the observed calibration data (Table 1). The

281 selection of parameters for optimization was based on formal sensitivity analysis
282 (Sargsyan et al., 2013) and prior experience with the model. We defined the sum of
283 squared errors (SSE) between simulation and observations weighted by data uncertainty
284 as the cost function for the optimization. We used a genetic algorithm (Runarsson and
285 Yao, 2000) to find a set of parameters that minimizes the cost function. Simulations were
286 performed in parallel using 2 populations of 32 ensemble members in parallel over 100
287 iterations for a total of 6400 model simulations.

288 For the pretreatment (pre-labeling) period, we compared the standard 'parameter'
289 version of the model (PRE-STD) with the optimized 'parameter' version (PRE-OPT).
290 The model with optimized parameters was used in simulations for the shading treatment
291 period for both the high shade and low shade treatments. Because of uncertainties
292 associated with simulated stomatal conductance and transpiration in high-shade
293 conditions, we performed additional parameter calibrations for the parameters mp (slope
294 of the Ball-Berry stomatal conductance formulation) and bp (intercept of the Ball-Berry
295 stomatal conductance formulation) during the shade treatment period using the genetic
296 algorithm with transpiration and stem growth data as constraints (HS_MB), with results
297 discussed below.

298 2.2.3 Evaluation of CLM photosynthesis functions

299 Since we are interested in understanding the fate of photosynthetically fixed carbon as it
300 is allocated to various tissues and fluxes, and how allocation dynamics respond to
301 changes in photosynthesis as driven by changes in PAR, it is useful to evaluate model
302 predictions of photosynthesis over a range of light levels. We used a functional unit
303 testing framework (Wang et al. 2014) to evaluate CLM's representation of the

304 photosynthetic light response at the scale of individual leaves against light-response
305 curves obtained by Warren et al. (2012) for foliage in the upper canopy of trees at the
306 PiTS experimental site prior to the shade treatment. This approach isolates the targeted
307 model process to allow a direct comparison between instrumental data and simulation
308 output, driving the model component with specified environmental conditions and
309 parameter values.
310

311 # 3 Results

312 ## 3.1 Environmental forcing conditions

313 Mean surface air temperature adjacent to the site decreased from days -20 to 4 (day
314 numbering is negative prior to the addition of $^{13}CO_2$ and shading treatments), then
315 recovered somewhat and remained without obvious trend for the rest of the post-labeling
316 period (days 5 to 25). Multiple rainfall events were recorded in the pre-treatment and
317 treatment periods (Fig. 2a). The shortwave and longwave radiation drivers for our
318 simulations, based on a combination of observations and estimation as described above,
319 showed variance associated with weather patterns during the experiment, with the
320 superimposed influence of the light and heavy shading treatments (Fig. 2b). $^{13}CO_2$
321 concentrations followed historical background values except during the labeling period
322 on day 0 (Fig. 2b).

323 ## 3.2 Pretreatment and treatment evaluation

324 The model predicted approximately exponential growth in all biomass pools during the 8
325 years of pretreatment simulation, with some evidence of slowing growth in the final years
326 (Fig. 3a). Using default global-scale ecophysiological parameters the model significantly

overestimated biomass accumulation in leaf, stem, and root pools, by 85%, 36%, and 76%, respectively on Sep. 1st of year 2010 (PRE_STD curves, Fig. 3a). Replacing default parameters with observed (lower) leaf N concentration and with calibrated (higher) allocation ratios for stem:leaf and root:leaf (complete set of parameter changes shown in Table 2) brought the biomass accumulation curves in better agreement with observations (Fig. 3a). Using the PRE_OPT parameters, the bias for leaf, stem, and root biomass accumulations was -9%, -4%, and -16%, respectively, compared to observed values.

Comparison of predicted vs. observed photosynthesis light response curves was used as an independent assessment of the model performance before and after calibration across a range of PAR values characteristic of mid-day values in the open field and under the LS and HS treatments (Fig. 3b). In the range of PAR from 750 to 1588 μmol m^{-2} s^{-1}, typical of mid-day conditions in the pre-treatment period (days -25 to -1), default parameterization (PRE_STD) resulted in overestimates of photosynthesis, while data-constrained and calibrated parameterization (PRE_OPT) eliminated the bias, placing predictions within +/- 1 SD of observed values. For light conditions characteristic of mid-day values in the LS treatment (648 +/- 232 μmol m^{-2} s^{-1}) the overprediction bias for the optimized model was reduced, but at least at PAR = 500 μmol m^{-2} s^{-1} the optimized model predicted photosynthesis was still biased high. For the range of PAR characteristic of the HS treatment (131 +/- 47 μmol m^{-2} s^{-1}) the model with optimized parameters underestimated photosynthesis, while the model with default parameters was in good agreement (low end of the range) or was biased high (high end of the HS range).

Soil temperature predicted by the optimized model at 0-5 cm depth had a consistent overestimation bias of 1-2 °C, but the model closely reproduced the daily

350 variation and decreasing tendency in near-surface soil temperature in both the
351 pretreatment and post-treatment periods (Fig. 4a). No clear influence of shading
352 treatments on soil temperature was seen in either the observations or model simulations.
353 Substantial variability in observed soil moisture (integrated for 15-95 cm depth) was
354 found among samples taken near different trees under the same shading treatment (Fig.
355 4b). Pretreatment observations of soil water content were not made, but observed LS soil
356 water was lower than that of the HS soil water at the start of the treatment period, perhaps
357 reflecting local differences in soil properties and pretreatment evapotranspiration.
358 Although modeled soil water content at the start of the treatment was higher than
359 observed (by 5-7%, measured as volume % of water in soil), the maximum observed and
360 simulated excursions in soil water content between rain events during the treatment
361 period were similar (4% and 3.5%, respectively). Predicted soil water content declined
362 more slowly than observed during days 16-25. There is some evidence of both observed
363 and predicted LS water content declining more rapidly than HS in this same period,
364 suggesting higher rates of evaporation for LS than HS.
365 Observed transpiration during the pretreatment period was higher for HS than LS
366 plots, likely a consequence of the higher biomass and leaf area of the HS trees (Warren et
367 al., 2012) and perhaps also higher soil water content (Fig. 4b). We used the pretreatment
368 transpiration data to calibrate CLM, and the model simulated the pretreatment
369 observations well in terms of both magnitude and temporal variations (Fig. 4c). After the
370 treatment initiation, decreased transpiration was seen in both observations and model
371 simulations for the HS and LS trees. For the LS case, CLM captured the observed
372 transpiration well. However in the HS case, CLM predicted a sharp reduction in

373 transpiration, whereas the observations differed relatively little from the LS case. To
374 investigate this difference further, we performed a second optimization for the Ball-Berry
375 stomatal conductance slope and intercept terms (HS_MB). However, despite increasing
376 these parameters to near the maximum acceptable values (Table 1), the HS_MB
377 optimization failed to reproduce the measured transpiration.
378 Both HS and LS trees showed increasing trend in stem carbon during the
379 pretreatment period, as inferred from stem thickness measurements. While the LS stems
380 continued to grow during the treatment period, the observed HS stem size declined (Fig.
381 5a). Modeled relative increase in stem carbon was more rapid during the pretreatment
382 period than observed, and while the modeled LS trees continued to accumulate carbon
383 during the treatment period (at a somewhat reduced rate) the modeled HS tree growth
384 essentially stopped. The observed shorter-term (3-5 day) variation in stem carbon (based
385 on diameter change) under shading (Fig. 5a) was attributed primarily to precipitation
386 events and changing soil moisture (Fig. 2a and Fig. 4b), and the accompanying swelling
387 and shrinkage of stem diameter, which translates through the allometric functions to
388 apparent changes in stem biomass. Apart from whole-plant mortality and fire, the model
389 has no physiological mechanisms allowing for negative growth of stems.
390 Both observed and simulated soil respiration tended to decline over the study
391 period (after Day-10 in the observations) (Fig. 5b). The observed pretreatment soil
392 respiration beneath the trees chosen for the HS treatment was 30% higher than under
393 those selected for the LS treatment. After the application of the shade treatments, relative
394 differences between the observed HS and LS soil respiration were reduced, but
395 respiration from HS soil remained higher. In contrast, simulated soil respiration was

slightly higher under LS, although the difference is quite small. The observed short-term variability in soil respiration under both HS and LS was not well simulated. While observations showed a reduced soil respiration coinciding with large precipitation events around Days -10, +10, and +15, simulated soil respiration rose on those days.

3.3 ^{13}C evaluation

Observations of foliar $\delta^{13}C$ show that LS and HS leaves acquired a similar concentration of labeled C, as intended by the experimental design (Fig. 6a). Observed appearance of the labeled C in phloem shows that photosynthate was rapidly moved out of leaves and into phloem, with peak observed phloem concentrations on day 2 for both LS and HS trees (Fig. 6b). Labeled C was observed in CO_2 at the soil surface, with peak concentrations around day 4 indicating a transfer through phloem to roots and metabolism belowground either as root respiration or as heterotrophic respiration of root exudate or root tissue (Fig. 6d). Increase in labeled C was observed in root tissue for both LS and HS trees, with large variability in measurements (Fig. 6c). Leaf, phloem, and root tissues showed remaining labeled C at day 20, and the label was still evident in soil surface CO_2 at day 15. For both phloem and soil surface CO_2, the LS plots showed lower label concentrations than the HS plots throughout the observed rise and fall of the labeled pulse. Differences between label dynamics for LS and HS roots are difficult to assess due to variability in measurements.

The model reproduced observed pretreatment values for foliar, phloem, and root tissue $\delta^{13}C$, and for $\delta^{13}C$ in soil CO_2 flux to within 1.5‰ (Fig. 6), indicating reasonable model parameterizations for ^{13}C discrimination through the stomatal conductance and photosynthesis pathways. The model allocation approach deploys new photosynthate

419 immediately throughout the plant to meet current maintenance and growth respiration
420 demands. The belowground component of the modeled autotrophic respiration is seen as
421 a large spike in labeled C in soil surface CO_2 on day 0. Other similar spikes were
422 simulated in association with respiration of aboveground plant parts (results not shown).
423 Lacking a representation for multi-day transport of photosynthate to sites of growth,
424 either acropetally towards new canopy growth or basipetally towards stem or root
425 growth, the model allocates labeled C to new growth pools immediately, where it is
426 considered well-mixed with the existing plant tissues. There was thus a rapid increase and
427 then a relative stabilization of the $\delta^{13}C$ label in foliage and root tissue. The model does
428 include storage pools, which hold photosynthate for deployment as new growth in
429 following growing seasons. Those pools were lumped for comparison to the phloem
430 observations (Fig. 6b), and they followed a pattern similar to the predicted leaf and root
431 tissue pools.
432 The model predicted a steady dilution of labeled C in leaf, root, and storage pools
433 for the LS trees, compared to their HS counterparts. With a severe reduction in PAR,
434 GPP was greatly reduced in the modeled HS treatment, and what little photosynthate
435 produced was prioritized for maintenance respiration, so the label appeared quickly in
436 tissues and remained relatively constant for that treatment. For the LS treatment GPP
437 remained relatively high following the labeling and initiation of the shade treatment. In
438 this case unlabeled C continued to accumulate as new growth, causing a steady decline in
439 the label concentration for LS trees over the course of the experimental period (Fig.
440 6a,b,c, insets). In contrast to the plant pools, modeled soil surface CO_2 shows a gradual
441 increase in label concentration after the initial root respiration pulse on day 0, with HS

consistently showing a higher concentration of label than LS for the simulated soil surface CO_2 through the end of the treatment period (Fig. 6d, inset). The modeled process of leaf and fine root litterfall is continuous throughout the year for evergreen vegetation, and this modeled rise in soil surface CO_2 concentration of labeled C is due to litterfall and subsequent metabolism by heterotrophs.

Toward the end of the experimental period, the observed multi-day pulses of labeled C in phloem and soil surface CO_2 approached the relatively stable values predicted by the model. The observed trajectory for label concentration in leaves fell below modeled values for the final ten days of treatment. Variation in observed root label concentration toward the end of the experiment makes it difficult to assess correspondence with model results for that tissue.

4 Discussion

4.1 Assessment of model performance in pretreatment period

Default model physiological parameters most appropriate to our site are based on averages taken across numerous datasets collected in evergreen needleleaf forests. There is considerable variation within that broad type classification for all of the measured parameters (White et al. 2000), and any time a site-level evaluation is used to assess model behavior (as here) it is helpful to constrain within this range according to the local species or species mixture. We used measurements taken directly from the site where available, and constrained the optimization of other parameters based on the observed ranges for loblolly pine, when available. The fine-root to leaf allocation ratio increased from 1.0 to 1.24, which is well within the range of reported values (White et al., 2000).

465 The fraction of leaf nitrogen in RuBisCO was 70% higher than the model default value,
466 and while on the high end, is consistent with measurements of other loblolly pine trees
467 (Tissue et al., 1995). The temperature sensitivity of maintenance respiration (Q_{10mr})
468 nearly doubled from the default value of 1.5 to 2.83. This is higher than most values in
469 the literature but is consistent with the value of 2.71 reported by Hamilton et al. (2001)
470 for loblolly pine, although this value only pertains to leaf respiration. The optimized
471 value for stem to leaf allocation ratio also is higher than in the default model, but it falls
472 well within the observed range for loblolly pine (White et al. 2000).

473 The optimized model delivered very reasonable simulations of pretreatment tree
474 biomass, transpiration, and leaf $\delta^{13}C$ (Figs. 3a, 4c, and 6a). Including multiple
475 independent observational metrics in the optimization cost function is a more challenging
476 test of correct model structure, compared to optimization targeting a single model output
477 variable (Sacks et al. 2006; Richardson et al., 2010; Ricciuto et al., 2011). The fact that
478 our optimized model delivers good results for all three components simultaneously
479 (biomass, transpiration, and leaf $\delta^{13}C$) supports the notion that stand-scale model
480 structure is reasonable.

481 Independent evaluation of model results at the leaf-scale demonstrated that the
482 optimized parameters either reduced biases (LS and open-field light levels) or gave
483 mixed results (HS light levels) at this scale. This provides additional confirmation that the
484 optimization approach was reasonable, and was not generating unrealistic parameter
485 values to compensate for gross structural deficiencies in the model. This is further
486 confirmed by the fact that optimized parameters (Table 1) controlling stomatal
487 conductance changed only modestly from default values.

488 Independent evaluation of model against pretreatment $\delta^{13}C$ in phloem and in soil
489 surface CO_2 shows good agreement, consistent with the targeted pretreatment value for
490 $\delta^{13}C$ in leaves. Simulated bulk root $\delta^{13}C$ is biased slightly high (Fig. 6c), indicating
491 possible errors in root turnover time, or the model's failure to account for post-
492 photosynthetic fractionation (Badeck et al., 2005).
493 Though several changes in the canopy photosynthesis scheme were made in the
494 version 4.5 of CLM (Bonan et al., 2011; Oleson et al., 2013), in this work, the canopy
495 photosynthesis process of CLM4.0 did a reasonably good job against our evaluation
496 metrics, including the leaf-level light response data. The ability of our optimized model
497 to reproduce pretreatment biomass, transpiration, ^{13}C discrimination, and leaf-scale
498 photosynthetic response to light gives confidence in the model's ability to simulate the
499 shading effect, and the model's ability to scale leaf-level processes to growth at the
500 whole-tree scale.

501 ## 4.2 Assessment of model performance in treatment period

502 We did not attempt to optimize model predictions for soil temperature or soil
503 moisture content. The model overestimation of soil temperature while faithfully
504 reproducing the multi-day excursions in temperature is consistent through the
505 pretreatment and treatment periods. Soil surface temperatures were not measured, so it is
506 not clear if the overestimation bias is related to a surface energy balance bias, to a bias in
507 the overlying air temperature, or to parameterization error in thermal diffusivity and its
508 relationship to soil texture and surface layer properties.
509 The overestimation bias in modeled soil moisture during the treatment period
510 (there were no pretreatment observations) suggests a parameterization error for soil

511 texture or variation in texture with depth. Small differences in the clay fraction, for
512 example, could cause the observed offset in mean soil water content, and clearly there is
513 variability in soil moisture states across the site, both within and between the shade
514 treatments (Fig. 4b). We used a single estimate of sand, silt, and clay fractions from the
515 site, and were satisfied that the model was able to capture pretreatment transpiration with
516 that soil parameterization, and that the multi-day excursions of soil moisture were of
517 similar magnitude in the model compared to observations during the treatment period.
518 We also note that modeled stomatal conductance was not impacted by lack of soil water
519 in these simulations. Periodic rainfall kept soils relatively wet throughout the pre-
520 treatment and treatment periods, minimizing effects of bias in soil moisture on simulated
521 photosynthesis or transpiration.
522 The very large difference between modeled and measured transpiration for the HS
523 treatment is the most confounding result from our study. All evidence indicates that the
524 model carbon and water dynamics are well-behaved for the pretreatment period, and the
525 model also captures the influence of light shading on transpiration accurately. Stem
526 growth results indicate that reduced growth of LS trees, and the cessation of growth for
527 HS trees, is captured properly by the model. Through the Ball-Berry approximation
528 linking stomatal conductance to photosynthetic rate, the model is forced into a state of
529 reduced transpiration for the HS treatment, even with additional optimization that placed
530 Ball-Berry parameters at their outer observational limits. It is possible that the sapflow
531 measurements in the HS treatment are biased, and that the actual tree-scale transpiration
532 is not as high as suggested by these measurements, but if true we would expect that bias
533 to occur for both pretreatment and treatment periods, and not only to appear in the

534 treatment period, as observed. Connected to that hypothesis, it is possible that actual leaf
535 stomatal conductance shut down during the HS treatment, but that water continued to
536 accumulate in the stem, moving past the sapflow sensors and filling a capacitance in the
537 xylem tissue. However, the sustained sapflow over the long duration of the treatment
538 period and the negative observed trend in stem diameter for HS trees argue against that
539 interpretation.

540 Alternatively, if we assume that the sapflow measurements reflect actual high
541 levels of transpiration in the HS trees, then we are forced to conclude that the Ball-Berry
542 relationship as implemented in CLM (De Kauwe et al., 2013; Oleson et al., 2010, 2013).
543 breaks down under these rather extreme experimental conditions. Under that hypothesis,
544 it would seem that there is some "memory" of the expected range of light levels in the
545 tree, and that even when photosynthesis is nearly extinguished due to experimentally
546 forced reduction in PAR, stomatal conductance remains at a relatively high level.
547 Another possibility is that these trees exhibit a strong nonlinearity in the relationship
548 between stomatal conductance and net photosynthesis, which has been observed at low
549 light levels and strongly impacts estimated transpiration (Barnard and Bauerle, 2013).
550 This type nocturnal transpiration may indeed have been greater for the HS trees if the
551 vapor pressure deficit was larger (Domec et al. 2012). Errors in modeled leaf temperature
552 and leaf boundary layer vapor pressure deficit may also contribute to the discrepancy
553 with observations. Conductance may have been maintained to some extent by vapor
554 pressure differences between the foliage and the shade cloth – indeed, dew was observed
555 on unshaded trees in early morning, yet not on the shaded trees. This hypothesis could be
556 tested in future studies with additional leaf-level measurements under HS treatments,

557 sampling both the diurnal cycle and the multi-day behavior of leaf physiology in trees
558 subjected to high levels of shading. While the HS conditions are unlikely to be realized
559 for extended periods under natural conditions, understanding this failure of the
560 commonly-used Ball-Berry parameterization may be helpful in understanding and
561 predicting the broader case of adaptation of stomatal behavior to environmental change,
562 which is known to influence water and carbon cycle predictions under future climates
563 (Damour et al., 2010).

564 Stem diameter can shrink or swell based on changes in stem xylem water content,
565 bark water content, and cambial growth, and is dependent on xylem water potential,
566 vapor pressure deficit, C availability, non-structural carbohydrate concentrations, and C
567 allocation (Vandegehuchte et al., 2014). C allocation to stem growth is revealed by a
568 step-wise increase in stem diameter that occurs in response to favorable conditions, and
569 that is maintained under less favorable conditions. The LS treatment clearly displayed the
570 step-wise increases in stem diameter, while the HS treatment displayed a reduction in
571 stem diameter. The shrinking stem diameter of HS trees indicates a decline in xylem and
572 phloem water content likely linked to phloem sugar concentration. The HS treatment
573 certainly reduced foliar C uptake and C available for phloem loading and allocation to
574 cambial growth (Warren et al., 2012).

575 The modeled difference between LS and HS in biomass accumulation in stems is
576 in good agreement with observations based on stem diameter, with increases of 1.9% and
577 1.6% by treatment day 19 for model and observations, respectively (Fig. 5a). Given the
578 previously discussed pretreatment results for biomass accumulation and leaf-scale
579 photosynthesis, we are confident in the optimized model's ability to capture carbon

580 dynamics at the plant scale on time scales of years to tens of days. It is reassuring to see
581 that the model prediction of soil respiration falls in the observed range, although this
582 could be the result of good luck as much as good performance. While soil respiration on
583 an annual basis is closely related to litter inputs and belowground plant respiration, it is
584 possible for compensating errors between decomposition rates and litter inputs, or
585 between litter inputs and root respiration, to result in good model-observation agreement
586 for the approximately monthly timescale examined here. We note a potential bias in the
587 model relationship between soil respiration and soil moisture: while the observed soil
588 respiration is depressed after large precipitation events, the model estimates an increase.
589 Neither CLM4's carbon allocation to roots nor its predicted root respiration is dependent
590 on soil water conditions. CLM4's heterotrophic contribution to soil respiration may also
591 have too little sensitivity and the timing of soil respiration response to soil water variation
592 may also be too simplistic. A more mechanistic treatment of water-air-microbe
593 interactions at the scale of soil pore space might help to eliminate these differences.
594 Resolved vertical transport of respired CO_2 in the soil column might also help to correct
595 this bias.

596 Beyond noting the obvious discrepancy in observed vs. modeled $\delta^{13}C$ dynamics
597 associated with the lack of short-term photosynthate storage pools in CLM, we are
598 interested in using this study to develop hypotheses explaining the observed patterns in
599 $\delta^{13}C$, identifying the simplest mechanisms that explain observed patterns, and
600 understanding the consequences of ignoring those mechanisms in a model like CLM. To
601 the extent that simple mechanisms can be identified, and significant consequences of
602 ignoring those mechanisms articulated, we leave it to future efforts to deploy and

603 evaluate those mechanisms in new model versions and with new observational and
604 experimental constraints.
605 Given that LS and HS leaves seem to have photosynthesized the pre-shading
606 labeled pulse of CO_2 at similar rates (Fig. 6a) as intended by the experimental design, we
607 can make some inferences about the dynamics of photosynthate storage and transport
608 based on the timing of the pulse as it exits the foliage and passes through the phloem of
609 the trunk, and based on differences in timing and concentration of the labeled pulse in LS
610 and HS trees. First, the fact that observed peak label concentration is higher in phloem
611 than in foliage, even though that peak comes two days later in phloem than in foliage,
612 indicates that the phloem pool in the vicinity of the labeling source (the leaf) is smaller
613 than the leaf pool itself. That is, even though the label is passing into the leaf prior to
614 entering the phloem, the label pulse is relatively small compared to the leaf carbon pool
615 as a whole, while it is relatively large compared to the part of the phloem pool nearest the
616 leaf at the time of labeling. Second, the observation that $\delta^{13}C$ in foliage declines rapidly
617 over the first ten days, and declines at about the same rate for LS and HS leaves, indicates
618 that the movement of newly-fixed photosynthate from leaves and into phloem does not
619 depend strongly on production of new photosynthate in subsequent days. Third, the
620 similar timing between LS and HS trees for peak label concentration in phloem, and later
621 in soil surface CO_2, indicates that the velocity of material movement through the phloem
622 does not depend strongly on current photosynthesis rate. Since the HS treatment clearly
623 reduced growth and transport belowground (Fig. 5), the logical conclusion is that the
624 cross-sectional area of active phloem tissue responsible for transport of photosynthate
625 away from leaves and out to roots is lower in the HS than in the LS treatment. One

626 possible interpretation is that the rate of flow within a given phloem pathway is relatively
627 constant, and that more phloem pathways towards the roots are active when production of
628 photosynthate is high. A logical consequence of that arrangement would be that at any
629 given point along the transport pathway towards the roots, or at any point in time at a
630 given location along the pathway, the concentration of a common-sized label would be
631 lower for a tree with high rate of ongoing photosynthesis than for a tree with low rate of
632 ongoing photosynthesis, due to dilution of the fixed-size label into a larger number
633 (larger cross-sectional area) of transport pathways, all with a common transport velocity
634 (conceptual model shown in Fig. 7). This is in fact the observed relationship of LS to HS
635 concentration at all points in time for both the phloem measurements (fixed point on the
636 trunk) and for the soil surface CO_2, lending support to the hypothesized mechanism.
637 Plant storage pools in the form of non-structural carbohydrates are known to play
638 an important role in regulating allocation to structural pools, and may make up a
639 significant portion of total biomass (e.g. Hoch et al., 2003). Simple models that account
640 for non-structural carbohydrates better compare with observed ^{14}C and stem growth,
641 indicating the importance of the pools over seasonal to decadal timescales (Richardson et
642 al., 2013). The question remains: What are the consequences for a CLM like model of
643 ignoring the shorter timescale (monthly) storage dynamics? (see Fig. 7). If we show that
644 the modeled and observed label concentrations tend to converge over monthly timescales,
645 we can argue that ignoring these short-term pools is not a first-order impediment to good
646 estimates of allocation and growth. Other more subtle aspects of the problem could,
647 however, have important implications for plot-scale and even global scale vegetation-soil
648 ecosystem dynamics and feedbacks. For example, the labeled soil surface CO_2 efflux is a

649 result from a combination of root respiration and heterotrophic respiration. The
650 heterotrophic component can be supplied by fresh litter inputs or by root exudation of
651 non-structural carbohydrate, which can be a significant fraction of net primary production
652 in some systems (Högberg et al., 2010). The difference between root mortality and root
653 exudation in terms of substrate quality, nutrient content, and interactions with soil
654 microbial communities could be very significant, especially as integrated over long
655 periods and under conditions of changing climate, changing atmospheric CO_2
656 concentration, and anthropogenic modifications to nutrient cycles.

657 Representing the existence and dynamics of short-term photosynthate storage
658 pools in a model like CLM could also help to resolve the mechanisms relating nutrient
659 mineralization and availability in soils with plant-microbe competition for available
660 nutrients and the influence of nutrient uptake on leaf-scale photosynthesis. In addition to
661 the shading treatments described here, other manipulations that would be useful to
662 explore include elevated CO_2 during and/or after the labeling pulse, imposed nutrient
663 limitations, and fertilization. Replicating these studies in other vegetation types would
664 help to assess the generality of storage pool structure and function, and would support
665 operational inclusion of these mechanisms in a global-scale model.

666 4.3 Implications for experimental design

667 Limitations identified in this first PiTS model-experiment interaction have already led to
668 improvements in follow-on experiments. For new experiments in a nearby dogwood
669 stand, additional observations include multiple treatments in different seasons, a
670 collection of absolute destructive tree biomass at the end of the study (rather than highly
671 uncertain estimates based on allometric relationships), seasonal leaf-level photosynthetic

672 measurements, assessment of mycorrhizal C flux, and improved meteorological
673 measurements. Although model parameters can be improved through optimization as in
674 this study, model parameters are being measured where possible. These additional
675 observational data are necessary for more detailed model evaluation and improvement of
676 model routines of C and allocation patterns at various time scales. Additional effort is
677 being devoted to characterizing the system prior to manipulation, including
678 measurements of biomass, soil physical and soil biogeochemical states.
679

680 # 5 Conclusions

681 The point version of CLM4 was implemented, calibrated and evaluated against carbon
682 and hydrology observations from a shading and labeling experiment in a stand of young
683 loblolly pines. We found that a combination of parameters measured on-site and
684 calibration targeting biomass, transpiration, and ^{13}C discrimination gave good agreement
685 with pretreatment measurements, including independent evaluation metrics at the leaf-
686 scale. We showed that the calibrated model captured the tree-scale and monthly temporal
687 dynamics of a light-shade treatment as it influenced carbon and water fluxes. The
688 calibrated model also captured the monthly time-scale carbon dynamics of a heavy-shade
689 treatment, but persistently estimated low levels of transpiration for the heavy-shade
690 treatment, while observed transpiration in that treatment remained nearly as high as for
691 the light-shade. We have suggested several possible explanations for the discrepancy, but
692 this remains a puzzling problem requiring further investigation.
693 Although the model lacks short-term photosynthate storage and transport
694 mechanisms that are clearly present in the real plants, first-order monthly time-scale

dynamics for carbon allocation and growth do not seem to suffer greatly. We used observations from the experiment to develop a conceptual model (hypothesis) of short-term photosynthate storage and transport, and suggested further studies that could be carried out to evaluate the generality of the hypothesized mechanisms. We suggested several research problems, which, if the proposed mechanism turns out to be generally valid, would benefit from model-experimental study in which the new mechanisms are incorporated into the model structure.

Acknowledgements. This work is supported by the US Department of Energy (DOE), Office of Science, Biological and Environmental Research. Oak Ridge National Laboratory is managed by UT-BATTELLE for DOE under contract DE-AC05-00OR22725.

References

Amthor, J. S., Chen, J. M., Clein, J. S., Frolking, S. E., Goulden, M. L., Grant, R. F., Kimball, J. S., King, A. W., McGuire, A. D., Nikolov, N. T., Potter, C. S., Wang, S., and Wofsy, S. C.: Boreal forest CO_2 exchange and evapotranspiration predicted by nine ecosystem process models: Intermodel comparisons and relationships to field measurements, J. Geophys. Res.-Atmos., 106, 33623-33648, 2001.

Arora, V. K., Boer, G. J., Friedlingstein, P., Eby, M., Jones, C. D., Christian, J. R., Bonan, G., Bopp, L., Brovkin, V., and Cadule P.: Carbon–concentration and carbon–climate feedbacks in CMIP5 Earth system models, J. Climate, 26, 5289-5314, 2013.

717 Atkin, O.: New phytologist and the ‘fate’ of carbon in terrestrial ecosystem, New Phytol,
718 205,1-3, 2015.
719 Badeck, F. W., Tcherkez, G., Nogues, S., Piel, C., and Ghashghaie, J.: Post-photo
720 synthetic fractionation of stable carbon isotopes between plant organs - a widespread
721 phenomenon, Rapid Commun Mass Sp, 19(11), 1381-1391, 2005.
722 Bahn, M., Buchmann, N., and Knohl, A.: Preface "Stable Isotopes and Biogeochemical
723 Cycles in Terrestrial Ecosystems", Biogeosciences, 9, 3979-3981, 2012.
724 Baldocchi, D., Falge, E., Gu, L., Olson, R., Hollinger, D., Running, S., Anthoni, P.,
725 Bernhofer, C., Davis, K., and Evans R.: FLUXNET: A new tool to study the temporal
726 and spatial variability of ecosystem-scale carbon dioxide, water vapor, and energy flux
727 densities, B. Am. Meteorol. Soc., 82, 2415-2434, 2001.
728 Baldwin, V. C. and Feduccia, D. P.: Loblolly pine growth and yield prediction for
729 managed west Gulf plantations, USDA For. Ser. Res. Pap., SO-236, New Orleans, LA:
730 U.S. Department of Agriculture, Forest Service, Southern Forest Experiment Station,
731 27 pp., 1987.
732 Barnard, D. M., and Bauerle, W. L.: The implications of minimum stomatal conductance
733 on modeling water flux in forest canopies, J. Geophys. Res.-Biogeo., 118, 1322-1333,
734 2013.
735 Bauerle, W. L., Oren, R., Way, D. A., Qian, S. S., Stoy, P. C., Thornton, P. E., Bowden,
736 J. D., Hoffman, F. M., and Reynolds, R. F.:, Photoperiodic regulation of the seasonal
737 pattern of photosynthetic capacity and the implications for carbon cycling, P. Natl.
738 Acad. Sci. USA, 109, 8612-8617, 2012.

739 Beer, C., Reichstein, M., Tomerlleri, E., Ciais, P., Jung, M., Carvalhai, N., Rodenbeck,
740 C., Arain, M. A., Baldocchi, D., Bonan, G. B., Bondeau, A., Cescatti, A., Lasslop, G.,
741 Lindroth, A., Lomas, M., Luyssaert, S., Margolis, H., Oleson, K. W., Roupsard, O.,
742 Veenendaal, E., Viovy, N., Williams, C., Woodward, F. I., and Papale, D.: Terrestrial
743 gross carbon dioxide uptake: global distribution and covariation with climate, Science,
744 329, 834-838, 2010.
745 Best, M. J., Pryor, M., Clark, D. B., Rooney, G. G., Essery, R. L. H., Menard, C. B.,
746 Edwards, J. M., Hendry, M. A., Porson, A., Gedney, N., Mercado, L. M. Sitch, S.,
747 Blyth, E., Boucher, O., Cox, P. M., Grimmond, C. S. B., and Harding, R. J.: The Joint
748 UK Land Environment Simulator (JULES), model description - Part 1: Energy and
749 water fluxes, Geosci. Model Dev., 4, 677-699, 2011.
750 Bonan, G. B., Hartman, M. D., Parton, W. J., and Wieder, W. R.: Evaluating litter
751 decomposition in earth system models with long-term litterbag experiments: an
752 example using the Community Land Model version 4 (CLM4), Glob. Change Biol.,
753 19, 957-974, 2013.
754 Bonan, G. B., Lawrence, P. J., Oleson, K. W., Levis, S., Jung, M., Reichstein, M.,
755 Lawrence, D. M., and Swenson, S. C.: Improving canopy processes in the Community
756 Land Model version 4 (CLM4) using global flux fields empirically inferred from
757 FLUXNET data, J. Geophys. Res.-Biogeo., 116 ,2011.
758 Bonan, G. B., Oleson, K. W., Fisher, R. A., Lasslop, G., and Reichstein, M.: Reconciling
759 leaf physiological traits and canopy flux data: Use of the TRY and FLUXNET
760 databases in the Community Land Model version 4, J. Geophys. Res.-Biogeo., 117,
761 2012.

762 Cannell, M. G. R. and Dewar R. C.: Carbon allocation in trees - a review of concepts for
763 modeling, Adv. Ecol. Res., 25, 59-104, 1994.
764 Dai, Y. J., Zeng, X. B., Dickinson, R. E., Baker, I., Bonan, G. B., Bosilovich, M. G.,
765 Denning, A. S., Dimeyer, P. A., Houser, P. A., Niu, G. Y., Oleson, K. W., Scholosser,
766 C. A., and Yang, Z., L.: The common land model, B. Am. Meteorol. Soc., 84, 1013-+,
767 doi: 10.1175/BAMS-84-8-1013, 2003.
768 Damour, G., Simonneau, T., Cochard, H., and Urban, L.: An overview of models of
769 stomatal conductance at the leaf level, Plant Cell Environ., 33, 1419-1438, 2010.
770 De Kauwe, M. G., Medlyn, B. E., Zaehle, S., Walker, A. P., Dietze, M. C., Hickler, T.,
771 Jain, A. K., Luo, Y. Q., Parton, W. J., Prentice, I. C., Smith, B., Thornton, P. E.,
772 Wang, S. S., Wang, Y. P., Warlind, D., Weng, E. S., Crous, K. Y., Ellsworth, D. S.,
773 Hanson, P. J., Seok Kim, H., Warren, J. M., Oren, R., and Norby R. J.,: Forest water
774 use and water use efficiency at elevated CO_2: a model-data intercomparison at two
775 contrasting temperate forest FACE sites, Glob. Change Biol., 19, 1759-1779, 2013.
776 De Kauwe, M. G., Medlyn, B. E., Zaehle, S., Walker, A. P., Dietze, M. C., Wang, Y. P.,
777 Luo, Y. Q., Jain, A. K., El-Masri, B., Hickler, T., Warlind, D., Weng, E. S., Parton, W.
778 J., Thornton, P. E., Wang, S. S., Prentice, I. C., Asao, S., Smith, B., McCarthy, H. R.,
779 Iversen, C. M., Hanson, P. J., Warren, J. M., Oren, R., and Norby, R. J.: Where does
780 the carbon go? A model–data intercomparison of vegetation carbon allocation and
781 turnover processes at two temperate forest free-air CO_2 enrichment sites, New Phytol.,
782 203, 883-899, 2014.
783 Domec J.C., Ogée J, Noormets A., Jouangy J. Gavazzi M., Treasure E., Sun G., McNulty
784 S. and J.S. King. 2012. Interactive effects of nocturnal transpiration and climate

785 change on the root hydraulic redistribution and carbon and water budgets of Southern
786 US pine plantations. Tree Physiology 32(6): 707-723.
787 Ehleringer, J. R., Buchmann, N., and Flanagan, L. B.: Carbon isotope ratios in
788 belowground carbon cycle processes, Ecological Applications, 10, 412-422, 2000.
789 Epron, D., Bahn, M., Derrien, D., Lattanzi, F. A., Pumpanen, J., Gessler, A., Hogberg, P.,
790 Maillard, P., Dannoura, M., Gerant, D., and Buchmann, N.: Pulse-labelling trees to
791 study carbon allocation dynamics: a review of methods, current knowledge and future
792 prospects, Tree Physiol., 32, 776-798, 2012.
793 Farquhar, G. D., J. R. Ehleringer, and K. T. Hubick: Carbon Isotope Discrimination and
794 Photosynthesis, Annu Rev Plant Phys, 40, 503-537, 1989.
795 Fox, A., Williams, M., Richardson, A. D., Cameron, D., Gove, J. H., Quaife, T., Ricciuto,
796 D., Reichstein, M., Tomelleri, E., Trudinger, C. M., and Van Wijk, M. T.: The
797 REFLEX project: Comparing different algorithms and implementations for the
798 inversion of a terrestrial ecosystem model against eddy covariance data, Agr. Forest
799 Meteorol., 149, 1597-1615, 2009.
800 Friedlingstein, P., Cox, P., Betts, R., Bopp, L., Von Bloh, W., Brovkin, V., Cadule, P.,
801 Doney, S., Eby, M., Fung, I., Bala, G., John, J., Jones, C., Joos, F., Kato, T.,
802 Kawamiya, M., Knorr, W., Lindsay, K., Matthews, H. D., Raddatz, T., Rayner, P.,
803 Reick, C., Roeckner, E., Schnitzler, K. G., Schnur, R., Strassmann, K., Weaver, A. J.,
804 Yoshikawa, C., and Zeng, N.: Climate-carbon cycle feedback analysis: Results from
805 the (CMIP)-M-4 model intercomparison, J. Climate, 19, 3337-3353, 2006.
806 Gent, P. R., Danabasoglu, G., Donner L. J., Holland, M. M., Hunke, E. C., Jayne, S. R.,
807 Lawrence, K. M., Neale, R. B., Rasch, P. J., Vertenstein, M., Worley P. H., Yang Z. L,

808 and Zhang, M. H.: The Community Climate System Model Version 4, J. Climate, 24,
809 4973-4991, 2011.
810 Griffin, K. L., Winner, W. E., and Strain, B. R.: Growth and dry matter partitioning in
811 loblolly and ponderosa pine seedlings in response to carbon and nitrogen availability,
812 New Phytol., 129, 547-556, 1995.
813 Hamilton, J. G., Thomas, R. B., and Delucia, E. H.: Direct and indirect effects of elevated
814 CO2 on leaf respiration in a forest ecosystem, Plant Cell Environ., 24, 975-982, 2001.
815 Hanson, P. J., Amthor, J. S., Wullschleger, S. D., Wilson, K. B., Grant, R. F., Hartley, A.,
816 Hui, D., Hunt, E. R., Johnson, D. W., Kimball, J. S., King, A. W., Luo, Y., McNulty,
817 S. G., Sun, G., Thornton, P. E., Wang, S., Williams, M. Baldocchi, D. D., and
818 Cushman, R. M.: Oak forest carbon and water simulations: Model intercomparisons
819 and evaluations against independent data, Ecol Monogr., 74, 443-489. 2004.
820 Hoch, G., Richter, A., and Korner, C.: Non-structural carbon compounds in temperate
821 forest trees, Plant Cell Environ, 26(7), 1067-1081, 2003.
822 Högberg, M. N., Briones, M. J. I., Keel, S. G., Metcalfe, D. B., Campbell, C., Midwood,
823 A. J., Thornton, B., Hurry, V., Linder, S., Näsholm, T., and Högberg, P.:
824 Quantification of effects of season and nitrogen supply on tree below-ground carbon
825 transfer to ectomycorrhizal fungi and other soil organisms in a boreal pine forest. *New*
826 *Phytol.* 187, 485-493, 2010.
827 Huntzinger, D. N., Post, W. M., Wei, Y., Michalak, A. M., West, T. O., Jacobson, A. R.,
828 Baker, I. T., Chen, J. M, Davis, K. J., Hayes, D. J., Hoffman, F. M., Jain, A. K., Liu,
829 S., McGuire, A. D., Neilson, R. P., Potter, C., Poulter, B., Price, D., Raczka, B. M.,
830 Tian, H. Q., Thornton, P. E., Tomelleri, E., Viovy, N., Xiao, J., Yuan, W., Zeng, N.,

831 Zhao, M., and Cook, R.: North American Carbon Program (NACP) regional interim
832 synthesis: Terrestrial biospheric model intercomparison, Ecol. Model., 232, 144-157,
833 2012.
834 Idso, S. B.: A set of equations for full spectrum and 8-mu-m to 14-mu-m and 10.5-mu-m
835 to 12.5-mu-m thermal-radiation from cloudless skies, Water Resour. Res., 17., 295-
836 304, 1981.
837 Keenan, T. F., Carbone, M. S., Reichstein, M., and Richardson, A. D.: The model-data
838 fusion pitfall: assuming certainty in an uncertain world, Oecologia, 167, 587-597,
839 2011.
840 Koven, C. D., Riley, W. J., Subin, Z. M., Tang, J. Y., Torn, M. S., Collins, W. D., Bonan,
841 G. B., Lawrence, D. M., and Swenson S. C.: The effect of vertically resolved soil
842 biogeochemistry and alternate soil C and N models on C dynamics of CLM4,
843 Biogeosciences, 10, 7109-7131, 2013.
844 Krinner, G., Viovy, N., de Noblet-Ducoudre, N., Ogee, J., Polcher, J., Friedlingstein, P.,
845 Ciais, P., Sitch, S., and Prentice, I. C.: A dynamic global vegetation model for studies
846 of the coupled atmosphere-biosphere system, Global Biogeochem. Cy., 19, 2005.
847 Lawrence, D. M., Oleson, K. W., Fanner, M. G., Thornton, P. E., Swenson, S. C.,
848 Lawrence, P. J., Zeng, X. B., Yang, Z. L., Levis, S., Sakaguchi, K., Bonan, G. B., and
849 Slater, A. G.: Parameterization improvements and functional and structural advances
850 in version 4 of the Community Land Model, J. Adv. Model Earth Sy., 3., M03001,
851 2011.
852 Li, H. Y., Huang, M. Y., Wigmosta, M. S., Ke, Y. H., Coleman, A. M., Leung, L. R.,
853 Wang, A. H., and Ricciuto, D. M.: Evaluating runoff simulations from the Community

854 Land Model 4.0 using observations from flux towers and a mountainous watershed, J.
855 Geophys. Res.-Atmos., 116, 2011.
856 Litton, C. M., Raich, J. W., and Ryan, M. G.: Carbon allocation in forest ecosystems,
857 Glob. Change Biol., 13, 2089-2109, 2007.
858 Luo, Y. Q., Randerson, J. T., Abramowitz, G., Bacour, C., Blyth, E., Carvalhais, N.,
859 Ciais, P., Dalmonech, D., Fisher, J. B., Fisher, R., Friedlingstein, P., Hibbard, K.,
860 Hoffman, F., Hunzinger, D., Jones, D. D., Koven, C., Lawrence, D., Li, D. J.,
861 Mahecha, M., Niu, S. L., Norby, R., Piao, S. L., Qi, X., Peylin, P., Prentice, I. C.,
862 Riley, W., Reichstein, M., Schwalm, C., Wang, Y. P., Xia, J. Y., Zaehle, S., and Zhou,
863 X. H.: A framework for benchmarking land models, Biogeosciences, 9, 3857-3874,
864 2012.
865 Mao, J. F., Shi, X. Y., Thornton, P. E., Piao, S. L., and Wang, X. H.: Causes of spring
866 vegetation growth trends in the northern mid-high latitudes from 1982 to 2004,
867 Environ. Res. Lett., 7, 014010, 2012a.
868 Mao, J. F., Thornton, P. E., Shi, X. Y., Zhao, M. S., and Post, W. M.: Remote sensing
869 evaluation of CLM4 GPP for the period 2000-09, J. Climate, 25, 5327-5342, 2012b.
870 Mao, J. F., Shi, X. Y., Thornton, P. E., Hoffman, F. M., Zhu, Z. C., and Myneni, R. B.:
871 Global latitudinal-asymmetric vegetation growth trends and their driving mechanisms:
872 1982-2009, Remote Sens.-Basel, 5, 1484-1497, 2013.
873 Naidu, S. L., DeLucia, E. H., and Thomas, R. B.: Contrasting patterns of biomass
874 allocation in dominant and suppressed loblolly pine, Can. J. Forest Res., 28, 1116-
875 1124, 1998.

876 Oleson, K., Lawrence, D. M., Bonan, G. B., Drewniak, B., Huang, M., Koven, C. D.,
877 Levis, S., Li, F., Riley, W. J., Subin, Z. M., Swenson, S., Thornton, P. E., Bozbiyik,
878 A., Fisher R.,. Heald, C. L, Kluzek, E., Lamarque, J. -F., Lawrence, P. J., Leung, L. R.,
879 Lipscomb, W., Muszala, S. P., Ricciuto, D. M., Sacks, W. J., Sun, Y., Tang, J., and
880 Yang, Z. -L.: Technical description of version 4.5 of the Community Land Model
881 (CLM), NCAR Technical Note NCAR/TN-503+STR, The National Center for
882 Atmospheric Research (NCAR): Boulder, CO, USA,420 pp., 2013.
883 Oleson, K. W., Lawrence, D. M., Gordon, B., Flanner, M. G., Kluzek, E., Lawrence, P.,
884 J., Levis, S., Swenson, S. C., Thornton, P. E., Dai, A., Decker, M., Dickinson, R.,
885 Feddema, J., Heald, C. L., Hoffman, F., Lamarque, J. –F., Mahowald, N., Niu, G. –Y.,
886 Qian, T., Randerson, J., Running, S., Sakaguchi, K., Slater, A., Stoeckli, R., Wang, A,
887 Yang, Z. –L., Zeng, X. D., and Zeng, X. B.: Technical description of version 4.0 of the
888 Community Land Model (CLM), NCAR Technical Note NCAR/TN 478+STR; The
889 National Center for Atmospheric Research (NCAR): Boulder, CO, USA, 257 pp.,
890 2010.
891 Oleson, K. W., Niu, G. –Y., Yang, Z. –L., Lawrence, D. M., Thornton, P. E., Lawrence,
892 P. J., Stoeckli, R., Dickinson, R. E., Bonan, G. B., Levis, S., Dai, A., and Qian, T.:
893 Improvements to the Community Land Model and their impact on the hydrological
894 cycle, J. Geophys. Res.-Biogeo., 113, G01021, 2008.
895 Ostle, N. J., Smith, P., Fisher, R., Woodward, F. I., Fisher, J. B., Smith, J. U., Galbraith,
896 D., Levy, P., Meir, P., McNamar, N. P., and Bardgett, R. D.: Integrating plant-soil
897 interactions into global carbon cycle models, J. Ecol., 97, 851-863, 2009.

898 Pitman, A. J.: The evolution of, and revolution in, land surface schemes designed for
899 climate models, Int. J. Climatol., 23, 479-510, 2003.
900 Raczka, B. M., Davis, K. J., Huntzinger, D., Neilson, R. P., Poulter, B., Richardson, A.
901 D., Xiao, J. F., Baker, I., Ciais, P., Keenan, T. F., Law, B., Post, W. M., Ricciuto, D.,
902 Schaefer, K., Tian, H. Q., Tomelleri, E., Verbeeck, H., and Viovy, N.:. Evaluation of
903 continental carbon cycle simulations with North American flux tower observations,
904 Ecol. Monogr., 83., 531-556, 2013.
905 Randerson, J. T., Hoffman, F. M., Thornton, P. E., Mahowald, N. M., Lindsay, K., Lee,
906 Y. H., Nevison, C. D., Doney, S. C., Bonan, G., Stoeckli, R., Covey, C., Running, S.
907 W., and Fung, I. Y.: Systematic assessment of terrestrial biogeochemistry in coupled
908 climate-carbon models, Glob. Change Biol., 15 2462-2484, 2009.
909 Ricciuto, D. M., King, A. W., Dragoni, D., and Post, W. M.: Parameter and prediction
910 uncertainty in an optimized terrestrial carbon cycle model: Effects of constraining
911 variables and data record length, J. Geophys. Res.-Biogeo., 116, 2011.
912 Richardson, A. D., Carbone, M. S., Keenan, T. F., Czimczik, C. I., Hollinger, D. Y.,
913 Murakami, P., Schaberg, P. G., and Xu X. M.: Seasonal dynamics and age of
914 stemwood nonstructural carbohydrates in temperate forest trees, New Phytol, 197(3),
915 850-861, 2013.
916 Richardson, A. D., Anderson, R. S., Arain, M. A., Barr, A. G., Bohrer, G., Chen, G. S.,
917 Chen, J. M., Ciais, P., Davis, K. J., Desai, A. R., Dietze, M. C., Dragoni, D., Garrity,
918 S. R., Gough, C. M., Grant, R., Hollinger, D. Y., Margolis, H. A., McCaughey, H.,
919 Migliavacca, M., Monson, R. K., Munger, J. W., Poulter, B., Raczka, B. M., Ricciuto,
920 D. M., Sahoo, A. K., Schaefer, K., Tian, H. Q., Vargas, R., Verbeeck, H., Xiao, J. F.,

921 and Xue, Y. K.: Terrestrial biosphere models need better representation of vegetation
922 phenology: results from the North American Carbon Program Site Synthesis, Glob.
923 Change Biol., 18, 566-584, 2012.
924 Richardson, A. D., Williams, M., Hollinger, D., Moore, D., Dail, D., Davidson, E., Scott,
925 N., Evans, R., Hughes, H., Lee, J., Ro- drigues, C., and Savage, K.: Estimating
926 parameters of a forest ecosystem C model with measurements of stocks and fluxes as
927 joint constraints, Oecologia, 164, 25–40, 2010.
928 Riley, W. J., Subin, Z. M., Lawrence, D. M., Swenson, S. C., Torn, M. S., Meng, L.,
929 Mahowald, N. M., and Hess, P.: Barriers to predicting changes in global terrestrial
930 methane fluxes: analyses using CLM4Me, a methane biogeochemistry model
931 integrated in CESM, Biogeosciences, 8, 1925-1953, 2011.
932 Runarsson, T. P., and Yao X.: Stochastic ranking for constrained evolutionary
933 optimization, IEEE T. Evolut. Comput., 4., 284-294, 2000.
934 Sargsyan, K., Safta, C., Habib, N. N., Debusschere, B. J., Ricciuto, D., and Thornton, P.
935 E.: Dimensionality reduction for complex models via bayesian compressive sensing,
936 Int. J. Uncertain. Quant., 4, 63-93, 2013.
937 Schaefer, K., Schwalm, C. R., Williams, C., Arain, M. A., Barr, A., Chen, J. M., Davis,
938 K. J., Dimitrov, D., Hilton, T. W., Hollinger, D. Y., Humphreys, E., Poulter, B.,
939 Raczka, B. M., Richardson, A. D., Sahoo, A., Thornton, P. E., Vargas, R., Verbeeck,
940 H., Anderson, R., Baker, I., Black T. A., Bolstad, P., Chen, J. Q., Curtis, P. S., Desai,
941 A. R., Dietze, M., Dragoni, D., Gough, C., Grant, R. F., Gu, L. H., Jain, A., Kucharik,
942 C., Law, B., Liu, S. G., Lokipitiya, E., Margolis, H. A., Matamala, R., McCaughey, J.
943 H., Monson, R., Munger, J. W., Oechel, W., Peng, C. H., Price, D. T., Ricciuto, D.,

944 Riley, W. J., Roulet, N., Tian, H. Q. Tonitto, C., Torn, M., Weng, e. S., and Zhou, X.
945 L.: A model-data comparison of gross primary productivity: Results from the North
946 American Carbon Program site synthesis, J. Geophys. Res.-Biogeo., 117, 2012.
947 Schimel, D. S., House, J. I., Hibbard, K. A., Bousquet, P., Ciais, P., Peylin, P., Braswell,
948 B. H., Apps, M. J., Baker, D., Bondeau, A., Canadell, J., Churkina, G., Cramer, W.,
949 Denning, A. S., Field, C. B. Friendlingstein, P., Goodale, C., Heimann, M., Houghton,
950 R. A., Melillo, J. M., Moore, B., Murdiyarso, D., Noble, I., Pacala, S. W., Prentice, I.
951 C., Raupach, M. R., Rayner, P. J., Scholes, R. J., Steffen, W. L., and Wirth, C.: Recent
952 patterns and mechanisms of carbon exchange by terrestrial ecosystems, Nature, 414,
953 169-172, 2001.
954 Schwalm, C. R., Williams, C. A., Schaefer, K., Anderson, R., Arain, M. A., Baker, I.,
955 Barr, A., Black, T. A., Chen, G. S., Chen, J. M., Ciais, P., Davis, K. J., Desai, A.,
956 Dietze, M., Dragoni, D., Fischer, M. L., Flanagan, L. B., Grant, R., Gu, L. H.,
957 Hollinger, D., Izaurralde, R. C., Kucharik, C., Lafleur, P., Law, B. E., Li, L. H., Li, Z.
958 P., Liu, S. G., Lokupitiya, E., Luo, Y. Q., Ma, S. Y., Margolis, H., Matamala, R.,
959 McCaughey, H., Monson, R. K., Oechel, W. C., Peng, C. H., Poulter, B., Price, D. T.,
960 Ricciuto, D. M., Riley, W., Sahoo, A. K., Sprintsin, M., Sun, J. F., Tian, H. Q.,
961 Tonitto, C., Verbeeck, H. and Verma, S. B.: A model-data intercomparison of CO_2
962 exchange across North America: Results from the North American Carbon Program
963 site synthesis, J. Geophys. Res.-Biogeo., 115, 2010.
964 Shi, X., Mao, J., Thornton, P. E., Hoffman, F. M., and Post, W. M.: The impact of
965 climate, CO2, nitrogen deposition and land use change on simulated contemporary
966 global river flow, Geophys. Res. Lett., 38, L08704, 2011.

967 Shi, X. Y., Mao, J. F., Thornton, P. E., and Huang, M. Y.: Spatiotemporal patterns of
968 evapotranspiration in response to multiple environmental factors simulated by the
969 Community Land Model, Environ. Res. Lett., 8, 024012, 2013.
970 Shi, X. Y., Thornton, P. E., Ricciuto, D. M., Hanson, P. J., Mao, J. F., Sebestyen, S. D.,
971 and Griffiths, N. A.: Capturing northern peatland microtopography and hydrology
972 within the Community Land Model, Biogeosciences Discuss., 12, 3381-3418, 2015.
973 Stoy, P. C., Dietze, M. C., Richardson, A. D., Vargas, R., Barr, A. G., Anderson, R. S.,
974 Arain, M. A., Baker, I. T., Black T. A., Chan, J. M., Cook, R. B., Gough, C. M., Grant,
975 R. F., Hollinger, D. Y., Izaurralde, R. C., Kucharik, C. J., Lafleur, P., Law, B. E., Liu,
976 S., Lokupitiya, E., Luo, Y., Munger, J. W., Peng, C., Poulter, B., Price, D. T.,
977 Ricciuto, D. M., Riley, W. J., Sahoo, A. K., Schaefer, K., Schwalm, C. R., Tian, H.,
978 Verbeeck, H., and Weng, E.: Evaluating the agreement between measurements and
979 models of net ecosystem exchange at different times and timescales using wavelet
980 coherence: an example using data from the North American Carbon Program Site-
981 Level Interim Synthesis, Biogeosciences, 10, 6893-6909, 2013.
982 Taylor, K. E., Stouffer, R. J., and Meehl, G. A.: An Overview of CMIP5 and the
983 Experiment Design, B. Am. Meteorol. Soc., 93, 485-498, 2012.
984 Tissue, D. T., Thomas, R. B., and Strain, B. R.: Growth and photosynthesis of loblolly
985 pine (*Pinus taeda*) after exposure to elevated CO_2 for 19 months in the field, Tree
986 Physiol., 16, 49-59,1995.
987 Thornton, P. E., and Rosenbloom, N. A.: Ecosystem model spin-up: Estimating steady
988 state conditions in a coupled terrestrial carbon and nitrogen cycle model, Ecol. Model.,
989 189, 25-48, 2005.

990 Thornton, P. E., Lamarque, J. F., Rosenbloom, N. A., and Mahowald, N. M.: Influence of
991 carbon-nitrogen cycle coupling on land model response to CO_2 fertilization and
992 climate variability, Global Biogeochem. Cy., 21, 2007.
993 Vandegehuchte, M. W., Guyot, A., Hubeau, M., De Swaef, T., Lockington, D. A., and
994 Steppe, K.: Modelling reveals endogenous osmotic adaptation of storage tissue water
995 potential as an important driver determining different stem diameter variation patterns
996 in the mangrove species *Avicennia marina* and Rhizophora stylosa, Ann. Bot., 114,
997 667-676, doi:10.1093/aob/mct311, 2014.
998 Vanlear, D. H., Taras, M. A., Waide, J. B., and Augspurger, M. K.: Comparison of
999 biomass equations for planted vs. natural loblolly-pine stands of sawtimber size, Forest
1000 Ecol. Manag., 14, 205-210, 1986.
1001 Walker, A. P., Hanson, P. J.., De Kauwe, M. G., Medlyn,B. E., Zaehle, S., Asao, S.,
1002 Dietze, M., Hickler, T., Huntingford, C., Iversen C. M., Jain, A., Lomas, M., Luo Y.,
1003 McCarthy, H., Parton, W. J., Prentice, I. C.., Thornton, P. E., Wang S., Wang, Y. –P.,
1004 Warlind, D., Weng, E., Warren, J. M., Woodward, F. I., Oren, R., and Norby, R. J.:
1005 Comprehensive ecosystem model-data synthesis using multiple data sets at two
1006 temperate forest free-air CO_2 enrichment experiments: Model performance at ambient
1007 CO_2 concentration, J. Geophys. Res. Biogeosci., 119, 937-964, 2014.
1008 Wang, D. L., Xu, Y., Thornton, P. E., King, A., Steed, C., Gu, L. H., and Schuchart, J.: A
1009 functional test platform for the Community Land Model, Environ. Modell. Softw., 55,
1010 25-31, 2014.

1011 Wang, Y. P., Kowalczyk, E., Leuning, R., Abramowitz, G., Raupach, M. R., Pak, B., van
1012 Gorsel, E., and Luhar, A.: Diagnosing errors in a land surface model (CABLE) in the
1013 time and frequency domains, J. Geophys. Res.-Biogeo., 116, 2011.
1014 Warren, J. M., Norby, R. J., and Wullschleger, S. D.: Elevated CO_2 enhances leaf
1015 senescence during extreme drought in a temperate forest, Tree Physiol., 31, 117-130,
1016 2011.
1017 Warren, J. M., Iversen, C. M., Garten, C. T., Norby, R. J., Childs, J., Brice, D., Evans, R.
1018 M., Gu, L., Thornton, P. E., and Weston, D. J.: Timing and magnitude of C
1019 partitioning through a young loblolly pine (Pinus taeda L.) stand using C-13 labeling
1020 and shade treatments, Tree Physiol., 32, 799-813, 2012.
1021 Warren, J. M., Iversen, C. M., Garten Jr., C. T., Norby, R. J., Childs, J., Brice, D., Evans,
1022 R. M., Gu, L., Thornton, P. E., and Weston, D. J.: PiTS-1: Carbon partitioning in
1023 loblolly pine after ^{13}C labeling and shade treatments, Carbon Dioxide Information
1024 Analysis Center, Oak Ridge National Laboratory, U.S. Department of Energy, Oak
1025 Ridge, Tennessee, U.S.A., doi: 10.3334/CDIAC/ornlsfa.001, 2013.
1026 White, M. A., Thornton P. E., Running S. W., and Nemani R. R.: Parameterization and
1027 sensitivity analysis of the BIOME-BGC terrestrial ecosystem model: net primary
1028 production controls, Earth Interactions, 4, 1–85, 2000.
1029 Williams, M., Richardson, A. D., Reichstein, M., Stoy, P. C., Peylin, P., Verbeeck, H.,
1030 Carvalhais, N., Jung, M., Hollinger, D. Y., Kattge, J., Leuning, R., Luo, Y., Tomelleri,
1031 E., Trudinger, C. M., and Wang, Y. –P.: Improving land surface models with
1032 FLUXNET data, Biogeosciences, 6, 1341-1359, 2009.
1033 Wullschleger, S. D., Hanson, P. J., and Todd, D. E.:Transpiration from a multi-species

1034 deciduous forest as estimated by xylem sap flow techniques, Forest Ecol. Manag., 143,
1035 205-213, 2001.
1036 Zaehle, S., Medlyn, B. E., De Kauwe, M. G., Walker, A. P., Dietze, M. C., Hickler, T.,
1037 Luo, Y. Q., Wang, Y. P., El-Masri, B., Thornton, P., Jain, A., Wang, S. S., Warlind,
1038 D., Weng, W. S., Parton, W., Iversen, C. M., Gallet-Budynek, A., McCarthy, H., Finzi,
1039 A. C., Hanson, P. J., Prentice, I. C., Oren, R. and Norby, R. J.: Evaluation of 11
1040 terrestrial carbon-nitrogen cycle models against observations from two temperate Free-
1041 Air CO_2 Enrichment studies, New Phytol., 202, 803-822, 2014.

Table 1.

Parameter	Description	Units	Default	PRE_OPT	HS_MB
measured					
slatop	Top of canopy specific leaf area (SLA)	m^2/gC	1.00E-02	1.02E-02	1.02E-02
dsladlai	Change in SLA through per unit LAI	gC^{-1}	1.25E-03	0	0
leafcn	leaf C:N ratio	gC/gN	35	50	50
optimized					
mp	Ball-Berry stomatal conductance slope	none	6	5.59	71.3
bp	Ball-Berry stomatal conductance intercept	$\mu mol\ m^{-2}\ s^{-1}$	5000	4960	61100
froot_leaf	fine root to leaf allocation ratio	none	1	1.24	1.24
stem_leaf	stem to leaf allocation ratio	none	2.2*	3.29	3.29
flnr	fraction of leaf N in RuBisCO	none	0.05	0.0845	0.0845
q10_mr	maintenance respiration t-sensitivity	none	1.5	2.83	2.83

*** stem-leaf allocation is a function of annual NPP. 2.2 is the nominal value at NPP = 800 gC m^{-2} yr^{-1}**

Table 2.

State variable	Units	Observed	PRE_STD	PRE_OPT	Bias reduction (%)
Leaf carbon	gC/m^2	[182,221]	419	209	96.55
Stem carbon	gC/m^2	[973,1220]	1455	1027	88.49
Root carbon	gC/m^2	488	859	408	78.44
Aboveground biomass	gC/m^3	[728,1758]	1645	1236	98.26
δ13C leaf	per mil	-27.99	-27.38	-27.49	18.03
δ13C phloem	per mil	-28.48	-27.38	-27.50	10.91
δ13C Root	per mil	-28.86	-27.36	-27.39	2.13
Sap flow	mm/day	2.40	3.70	2.37	97.85
Soil respiration	$\mu mol\ m^{-2}\ s^{-1}$	3.63	5.20	3.26	76.58

Captions of Tables and Figures

Table 1. Default PFT-level, site-specific and optimized parameters for the PiTS site used in CLM 4.0. PFT-level parameters are for the temperate evergreen needleleaf forest (ENF) type. Optimized values were obtained using the pretreatment data (PRE_OPT), and for the transpiration data during the shading period (HS_MB). In the HS_MB optimization, only the mp and bp parameters were optimized, while other parameters retain their pretreatment optimization values.

Table 2. Pretreament state variables included in the optimization. Simulated values were obtained using the default parameters (PRE_STD) and the optimized parameters (PRE_OPT). The bias reduction (%) caused by the optimization is listed in the last

1059 column. In the case of leaf, root and aboveground biomass, we use allometric equations
1060 from multiple sources (Baldwin, 1987; Naidu et al., 1998; Vanlear et al., 1986) that went
1061 into producing a range. The bias calculation uses the mean of the range. For sap flow and
1062 soil respiration, daily observations were made, but the values represent a mean over the
1063 25 pretreatment days over both LS and HS periods. $\delta^{13}C$ values represent observed and
1064 simulated values on the day before treatments began.
1065 **Figure 1** (a) Air temperature (T, °C), relative humidity (Hr, %) and (b) wind speed (u, m
1066 s^{-1}) under the shade cloth at the top of the canopy compared with open field
1067 measurements at 2 m height; (c) Typical diurnal patterns of photosynthetically active
1068 radiation (PAR, μmol m^{-2} s^{-1}) at the site under full sun, light shade or heavy shade
1069 treatments.
1070 **Figure 2** (a) Daily air temperature (°C) and precipitation (mm d^{-1}) for the pretreatment
1071 and treatment of light shade (LS) and heavy shade (HS) (Day -20 to 25), (b) change in
1072 daily atmospheric long wave radiation (LW, W m^{-2}), short wave radiation (SW, W m^{-2})
1073 and $^{13}CO_2$ (PPMV) prior to and after exposure to shade treatments. Dashed gray line
1074 represents the starting day of the treatment.
1075 **Figure 3** (a) CLM simulated change of leaf carbon (PRE_STD_LeafC), stem carbon
1076 (PRE_STD_StemC) and root carbon (PRE_STD_RootC) with default parameters, and
1077 change of those (PRE_OPT_LeafC, PRE_OPT_StemC and PRE_OPT_RootC) simulated
1078 with optimized parameters for the pretreatment period between year 2003 and Sep. 1st
1079 (dashed gray line) of year 2010. Observational estimations of leaf (OBS_LeafC, which
1080 are 221.1 g C m^{-2}, 283.8 g C m^{-2} and 181.9 g C m^{-2}), stem (OBS_StemC, which are
1081 1011.2 g C m^{-2}, 973.8 g C m^{-2} and 1220.1 g C m^{-2}) and root (OBS_RootC, which is 488.4

1082 g C m^{-2}) are based on measured stem diameters at breast height and allometric
1083 relationships from similarly aged loblolly pine (Baldwin, 1987; Naidu et al., 1998;
1084 Vanlear et al., 1986). Note that y-axis is log10-scaled. (b) Comparison of observed and
1085 simulated light response of top of the canopy leaves of loblolly pine at the PiTS-1 site.
1086 Solid black circles are mean ± 1 std dev of observations. Solid red and green circles are
1087 simulated results from the net photosynthesis module of the functional unit testing
1088 framework using site-observed parameters (PRE_STD) and optimized parameters
1089 (PRE_OPT), respectively (see section 2.2.2). Simulations are with the mean observed
1090 internal CO_2 concentrations (Ci) and leaf temperatures (Tleaf) at the observed light
1091 (PAR) levels and the site's observed leaf nitrogen (Na). Three grey bars represent the
1092 mean ± 1 std dev of midday PAR levels under the light shade treatment (LS), heavy
1093 shade treatment (HS) and open field condition (OF).
1094 **Figure 4** (a) Observed (obs) and CLM simulated (sim) daily soil temperature at 0-5cm
1095 depth (standard deviation, *SD* = 0.6-1.4 °C), (b) volumetric soil water content at 15-95cm
1096 depth (±*SD*) and (c) the transpiration before and after initiation of light shade (LS) or
1097 heavy shade (HS) treatments (*SD* = 0.1-1.7 mm day^{-1}). "HS – opt" represents the CLM
1098 simulation with optimized leaf conductance parameters. The vertical dashed lines
1099 indicate the starting day of the shade treatments.
1100 **Figure 5** (a) Observed (obs) and CLM simulated (sim) daily stem carbon relative to day
1101 0 (±*SD*), and (b) soil respiration prior to and after exposure to light shade (LS) and heavy
1102 shade (HS) treatments (±*SD*). Both observed and simulated stem carbon were normalized
1103 to 1 at Day 0. The simulated soil respiration is the combination of autotrophic respiration

1104 from roots and heterotrophic respiration from the decay of litter and soil organic matter.
1105 The vertical dashed lines indicate the starting day of the treatments.
1106 **Figure 6** (a) Observed (black) and CLM simulated (blue) change in $\delta^{13}C$ (parts per
1107 thousand (‰)) of (a) leaf, (b) phloem, (c) bulk root and (d) soil surface efflux $\delta^{13}C$ for the
1108 light shade (LS, open circle) and heavy shade (HS, filled circle) pretreatment and
1109 treatment periods (± standard error (SE)). The modeled $\delta^{13}C$ values were calculated from
1110 the CLM simulated ^{13}C and ^{12}C variables and the reference standard (0.0112372) using
1111 the equation described in https://en.wikipedia.org/wiki/Δ13C. The $^{13}CO_2$ labeling pulse
1112 was initiated on Sep. 1st in year 2010 (Day 0). Dashed gray line represents the starting
1113 day (again Day 0) of the shading treatment. To better visualize the model results, inset
1114 figures illustrate the CLM simulated $\delta^{13}C$ values for the light shade (open triangle) and
1115 heavy shade (filled triangle) treatments from Day 1 to Day 25.
1116 **Figure 7**. Conceptual model of label transport, assuming a constant velocity (V) of
1117 phloem stream with a cross-sectional area for the phloem pathway that varies as a
1118 function of ongoing photosynthetic rate. Cross-sectional area is conceptualized here as a
1119 varying number of similar phloem elements, with white elements in an active state, and
1120 dark elements inactive. The experimental case with a higher photosynthetic rate for the
1121 LS treatment and lower photosynthetic rate for the HS treatment is illustrated. Flux from
1122 roots (FR) includes root respiration, root exudation, and turnover of root tissue. The
1123 entire label is assumed to exit the leaf and enter the active phloem stream, at a rate that is
1124 independent of the ongoing rate of photosynthesis, as observed in the experiment.
1125

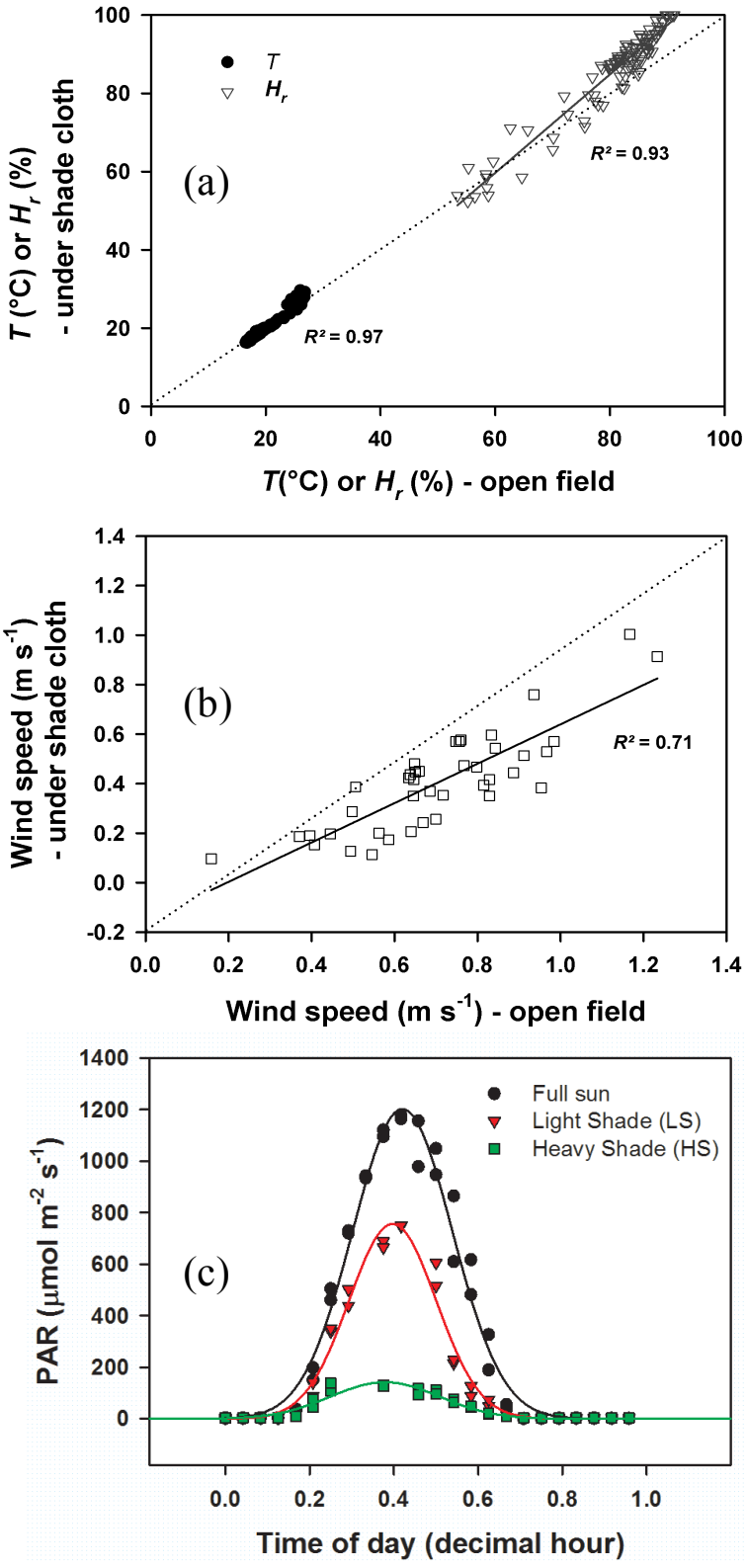

Figure 1 (a) Air temperature (T, °C), relative humidity (Hr, %) and (b) wind speed (u, m s^{-1}) under the shade cloth at the top of the canopy compared with open field measurements at 2 m height; (c) Typical diurnal patterns of photosynthetically active radiation (PAR, µmol m^{-2} s^{-1}) at the site under full sun, light shade or heavy shade treatments.

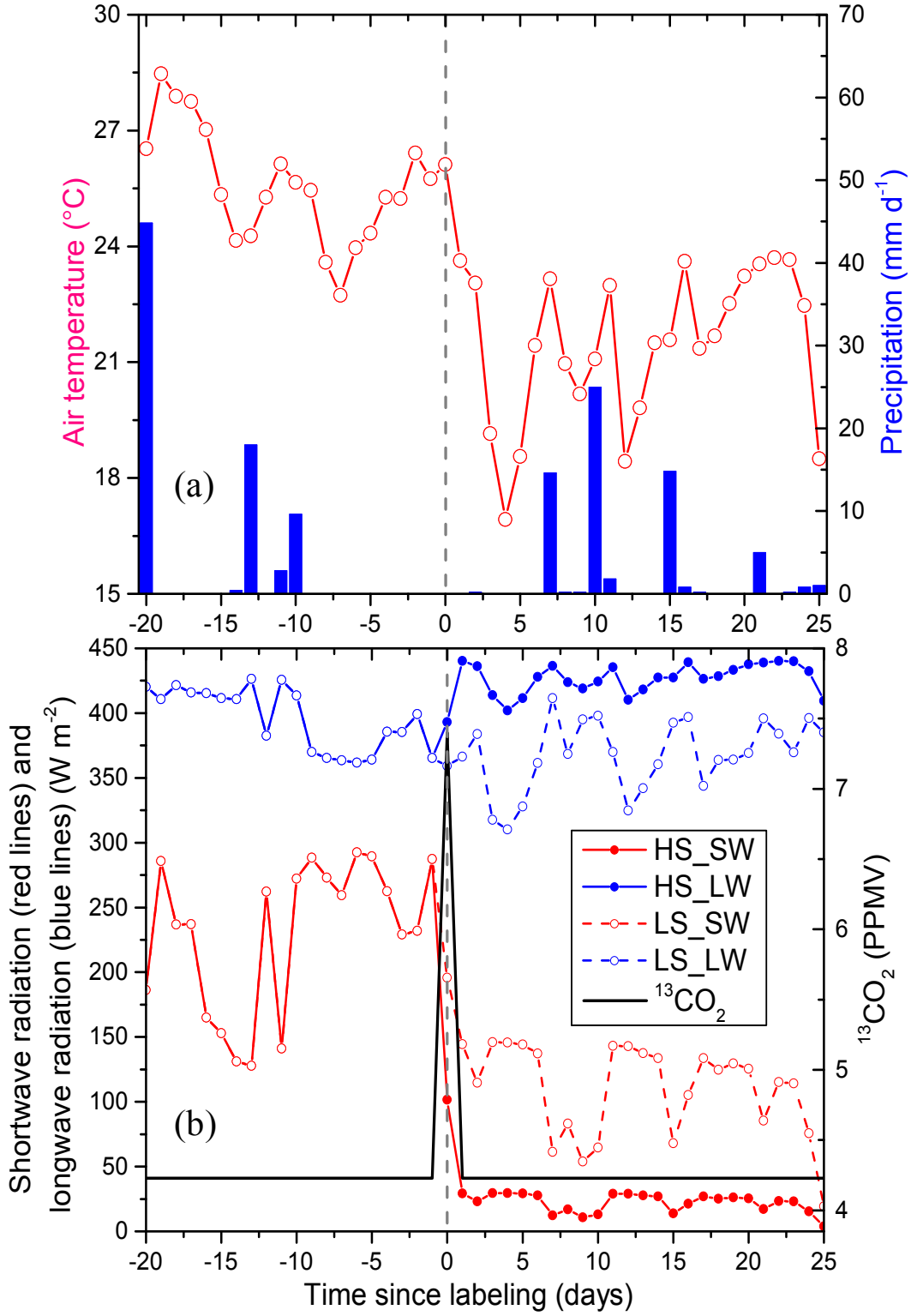

Figure 2 (a) Daily air temperature (°C) and precipitation (mm d^{-1}) for the pretreatment and treatment of light shade (LS) and heavy shade (HS) (Day -20 to 25), (b) change in daily atmospheric long wave radiation (LW, W m^{-2}), short wave radiation (SW, W m^{-2}) and $^{13}CO_2$ (PPMV) prior to and after exposure to shade treatments. Dashed gray line represents the starting day of the treatment.

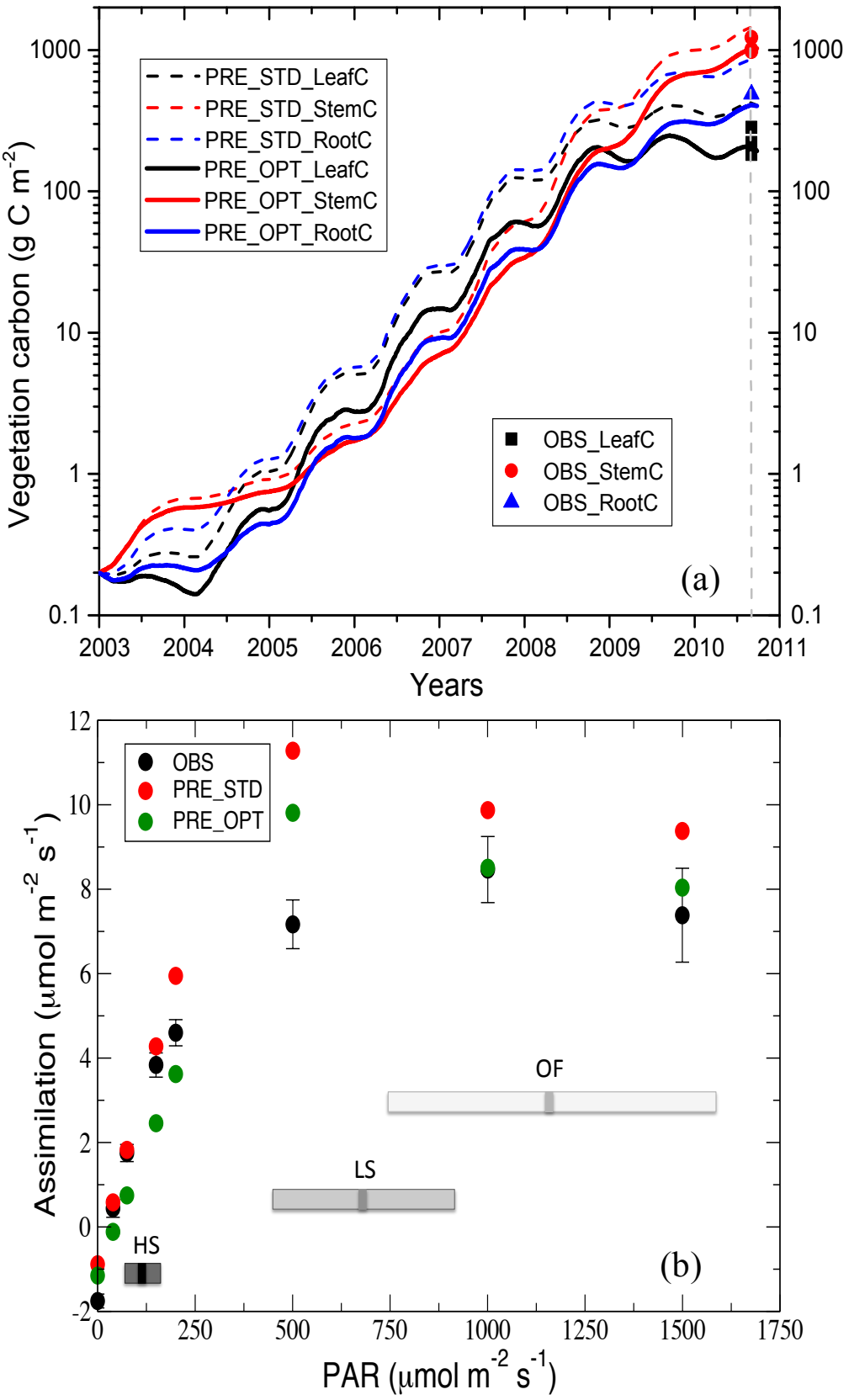

Figure 3 (a) CLM simulated change of leaf carbon (PRE_STD_LeafC), stem carbon (PRE_STD_StemC) and root carbon (PRE_STD_RootC) with default parameters, and change of those (PRE_OPT_LeafC, PRE_OPT_StemC and PRE_OPT_RootC) simulated with optimized parameters for the pretreatment period between year 2003 and Sep. 1st

(dashed gray line) of year 2010. Observational estimations of leaf (OBS_LeafC, which are 221.1 g C m^{-2}, 283.8 g C m^{-2} and 181.9 g C m^{-2}), stem (OBS_StemC, which are 1011.2 g C m^{-2}, 973.8 g C m^{-2} and 1220.1 g C m^{-2}) and root (OBS_RootC, which is 488.4 g C m^{-2}) are based on measured stem diameters at breast height and allometric relationships from similarly aged loblolly pine (*Baldwin*, 1987; *Naidu et al.*, 1998; *Vanlear et al.*, 1986). Note that y-axis is log10-scaled. (b) Comparison of observed and simulated light response of top of the canopy leaves of loblolly pine at the PiTS-1 site. Solid black circles are mean ± 1 std dev of observations. Solid red and green circles are simulated results from the net photosynthesis module of the functional unit testing framework using site-observed parameters (PRE_STD) and optimized parameters (PRE_OPT), respectively (see section 2.2.2). Simulations are with the mean observed internal CO_2 concentrations (Ci) and leaf temperatures (Tleaf) at the observed light (PAR) levels and the site's observed leaf nitrogen (Na). Three grey bars represent the mean ± 1 std dev of midday PAR levels under the light shade treatment (LS), heavy shade treatment (HS) and open field condition (OF).

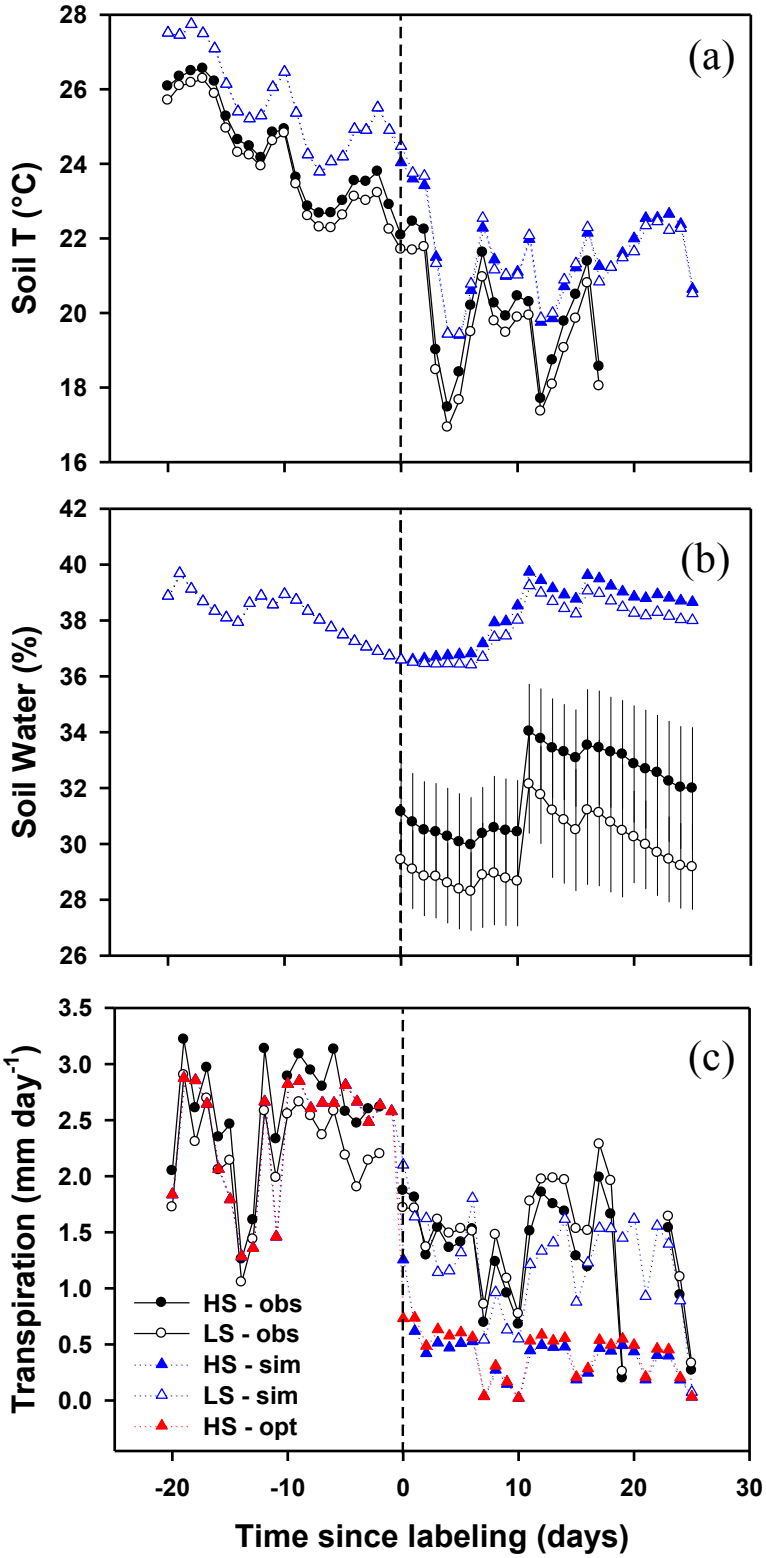

Figure 4 (a) Observed (obs) and CLM simulated (sim) daily soil temperature at 0-5cm depth (standard deviation, *SD* = 0.6-1.4 °C), (b) volumetric soil water content at 15-95cm depth (±*SD*) and (c) the transpiration before and after initiation of light shade (LS) or heavy shade (HS) treatments (*SD* = 0.1-1.7 mm day^{-1}). "HS – opt" represents the CLM simulation with optimized leaf conductance parameters. The vertical dashed lines indicate the starting day of the shade treatments.

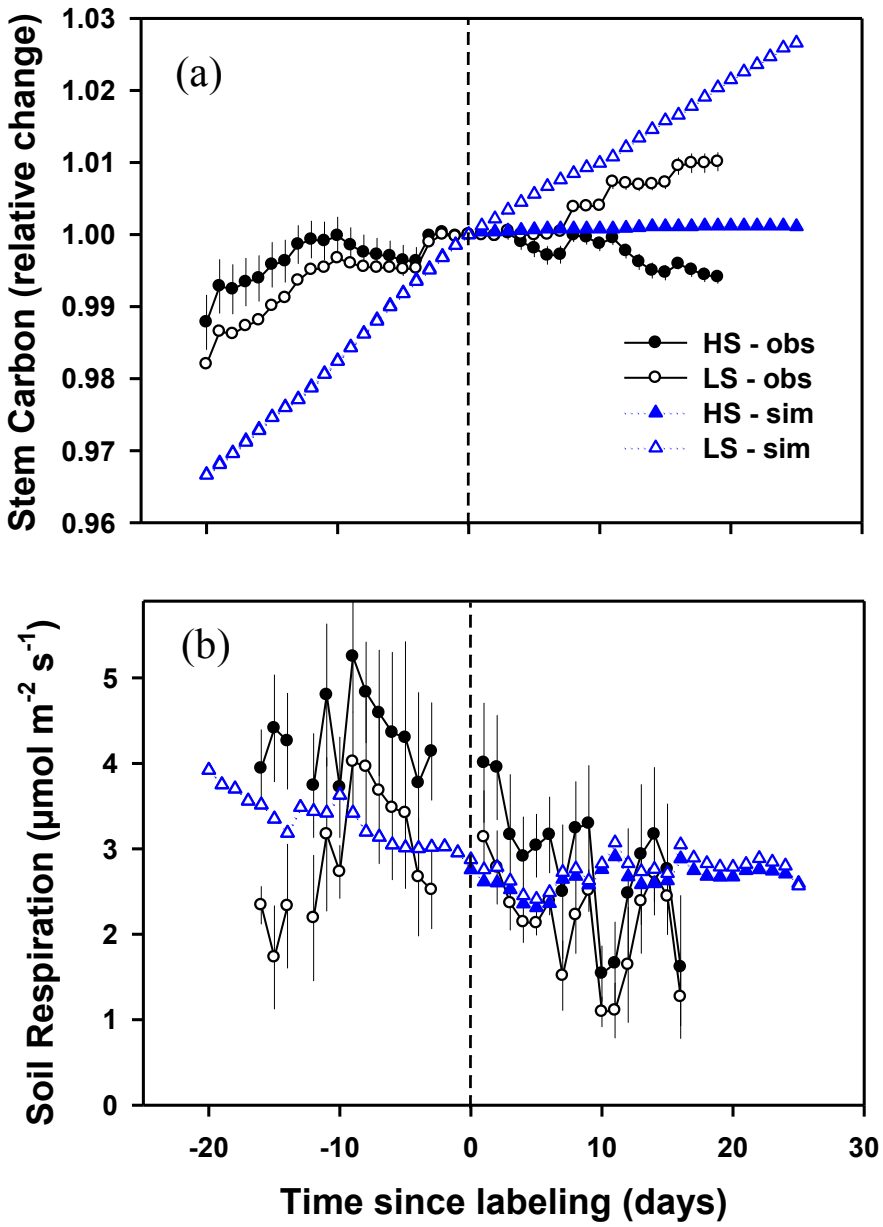

Figure 5 (a) Observed (obs) and CLM simulated (sim) daily stem carbon relative to day 0 (±*SD*), and (b) soil respiration prior to and after exposure to light shade (LS) and heavy shade (HS) treatments (±*SD*). Both observed and simulated stem carbon were normalized to 1 at Day 0. The simulated soil respiration is the combination of autotrophic respiration from roots and heterotrophic respiration from the decay of litter and soil organic matter. The vertical dashed lines indicate the starting day of the treatments.

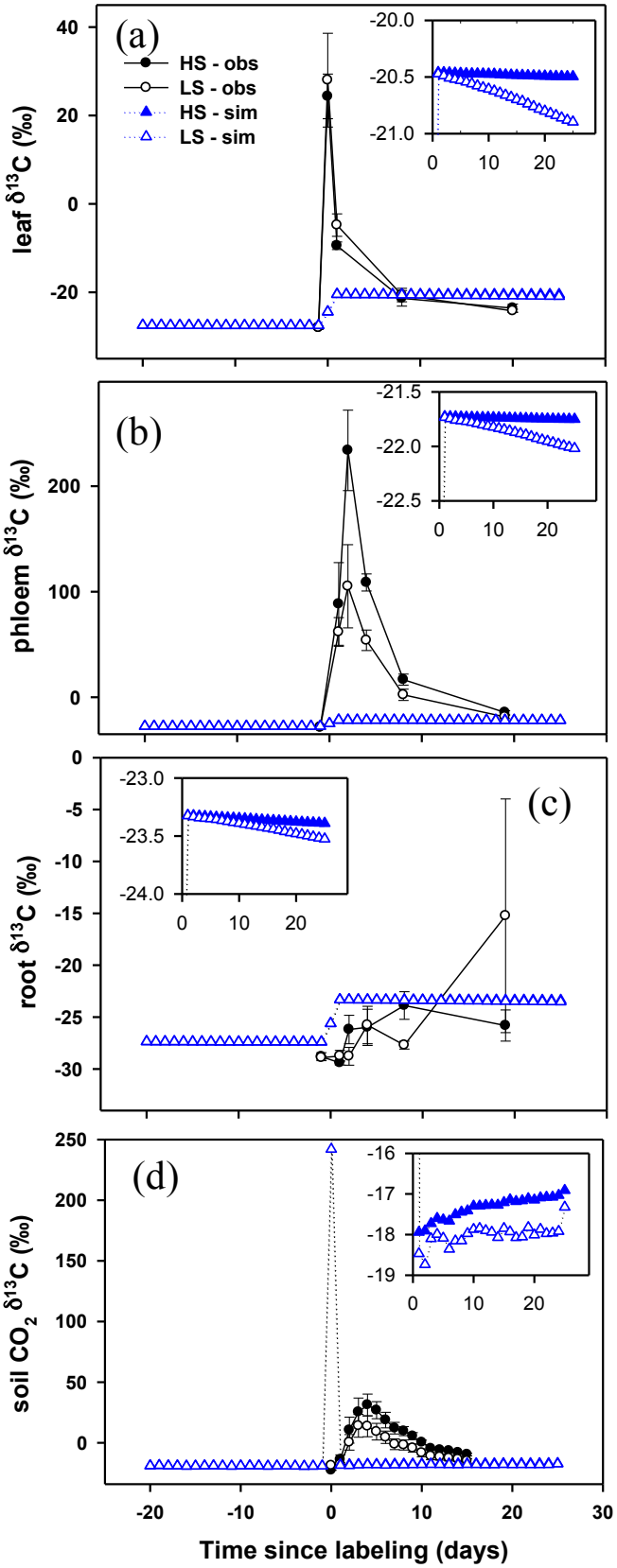

Figure 6 (a) Observed (black) and CLM simulated (blue) change in $\delta^{13}C$ (parts per thousand (‰)) of (a) leaf, (b) phloem, (c) bulk root and (d) soil surface efflux $\delta^{13}C$ for the light shade (LS, open circle) and heavy shade (HS, filled circle) pretreatment and treatment periods (± standard error (SE)). The modeled $\delta^{13}C$ values were calculated from the

CLM simulated ^{13}C and ^{12}C variables and the reference standard (0.0112372) using the equation described in https://en.wikipedia.org/wiki/Δ13C. The $^{13}CO_2$ labeling pulse was initiated on Sep. 1st in year 2010 (Day 0). Dashed gray line represents the starting day (again Day 0) of the shading treatment. To better visualize the model results, inset figures illustrate the CLM simulated $\delta^{13}C$ values for the light shade (open triangle) and heavy shade (filled triangle) treatments from Day 1 to Day 25.

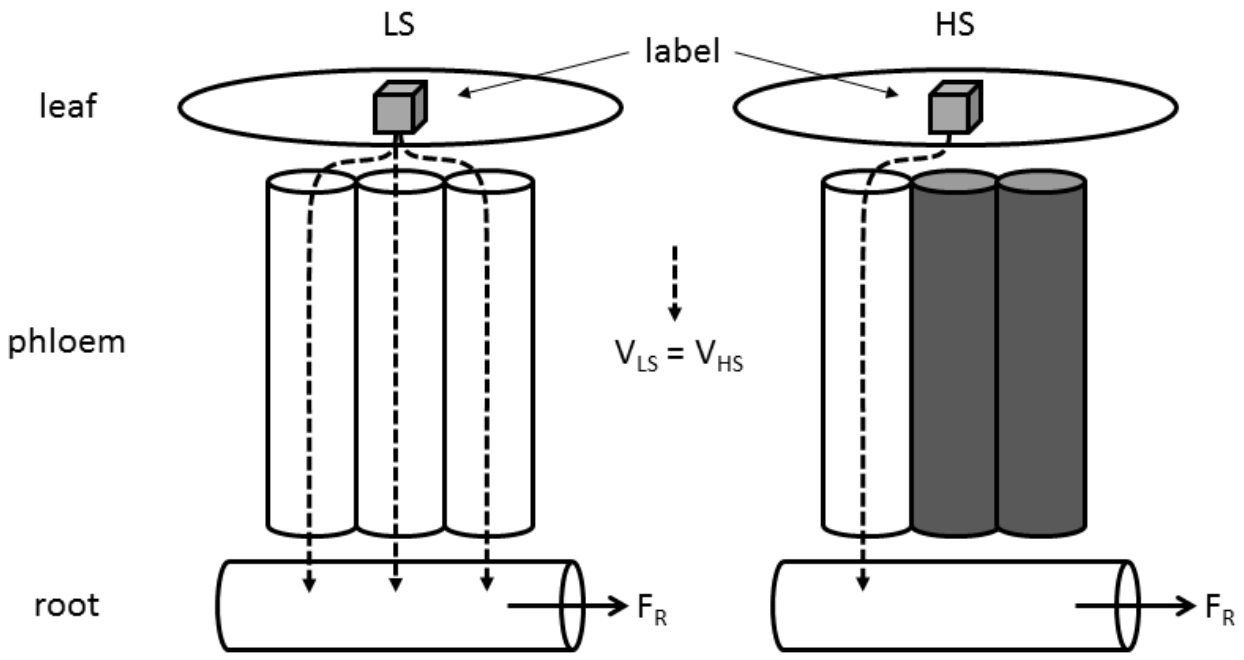

Figure 7. Conceptual model of label transport, assuming a constant velocity (V) of phloem stream with a cross-sectional area for the phloem pathway that varies as a function of ongoing photosynthetic rate. Cross-sectional area is conceptualized here as a varying number of similar phloem elements, with white elements in an active state, and dark elements inactive. The experimental case with a higher photosynthetic rate for the LS treatment and lower photosynthetic rate for the HS treatment is illustrated. Flux from roots (FR) includes root respiration, root exudation, and turnover of root tissue. The entire label is assumed to exit the leaf and enter the active phloem stream, at a rate that is independent of the ongoing rate of photosynthesis, as observed in the experiment.